Publication Year	2020
Acceptance in OA	2021-09-27T08:50:54Z
Title	Analysis of full disc Ca II K spectroheliograms III. Plage area composite series covering 1892-2019
Authors	CHATZISTERGOS, THEODOSIOS, ERMOLLI, Ilaria, Krivova, Natalia A., Solanki, Sami K., Banerjee, Dipankar, Barata, Teresa, Belik, Marcel, Gafeira, Ricardo, Garcia, Adriana, Hanaoka, Yoichiro, Hegde, Manjunath, Klimeš, Jan, Korokhin, Viktor V., Lourenço, Ana, Malherbe, Jean-Marie, Marchenko, G., Peixinho, Nuno, Sakurai, Takashi, Tlatov, Andrey G.
Publisher's version (DOI)	10.1051/0004-6361/202037746
Handle	http://hdl.handle.net/20.500.12386/31055
Journal	ASTRONOMY & ASTROPHYSICS
Volume	639

Analysis of full-disc Ca II K spectroheliograms

III. Plage area composite series covering 1892–2019*

eodosios Chatzistergos[1,2], Ilaria Ermolli[1], Natalie A. Krivova[2], Sami K. Solanki[2,3], Dipankar Banerjee
esa Barata[6], Marcel Belik[7], Ricardo Gafeira[6,8], Adriana Garcia[6], Yoichiro Hanaoka[9], Manjunath Hegd
n Klimeš[7], Viktor V. Korokhin[10], Ana Lourenço[6], Jean-Marie Malherbe[11,12], Gennady P. Marchenko
Nuno Peixinho[6], Takashi Sakurai[9], and Andrey G. Tlatov[13]

INAF Osservatorio Astronomico di Roma, Via Frascati 33, 00078 Monte Porzio Catone, Italy
e-mail: `theodosios.chatzistergos@inaf.it`
Max Planck Institute for Solar System Research, Justus-von-Liebig-weg 3, 37077 Göttingen, Germany
e-mail: `chatzistergos@mps.mpg.de`
School of Space Research, Kyung Hee University, Yongin, Gyeonggi 446-701, Republic of Korea
Indian Institute of astrophysics, Koramangala, Bangalore 560034, India
Aryabhatta Research Institute of Observational Sciences, Nainital 263 001, Uttarakhand, India
Univ Coimbra, CITEUC - Center for Earth and Space Research of the University of Coimbra, Geophysical and Astronomi
Observatory, 3040-004 Coimbra, Portugal
Observatory Upice, U lipek 160, 542 32 Úpice, Czech republic
Instituto de Astrofísica de Andalucía (CSIC), Apartado de Correos 3004, 18080 Granada, Spain
National Astronomical Observatory of Japan 2-21-1 Osawa, Mitaka, Tokyo 181-8588, Japan
Astronomical Institute of Kharkiv V.N. Karazin National University, 35 Sumskaya St., Kharkiv 61022, Ukraine
LESIA, Observatoire de Paris, 92195 Meudon, France
PSL Research University, Paris, France
Kislovodsk Mountain Astronomical Station, Central Astronomical Observatory, Russian Academy of Sciences, Kislovodsk,
Russia

eived 14 February 2020 / Accepted 4 May 2020

ABSTRACT

ntext. Studies of long-term solar activity and variability require knowledge of the past evolution of the solar surface magnetis
archives of full-disc Ca II K observations that have been performed more or less regularly at various sites since 1892 can se
n important source of such information.
s. We derive the plage area evolution over the last 12 solar cycles by employing data from all Ca II K archives that are publi
ilable in digital form, including several as-yet-unexplored Ca II K archives.
thods. We analysed more than 290 000 full-disc Ca II K observations from 43 datasets spanning the period between 1892–20
images were consistently processed with an automatic procedure that performs the photometric calibration (if needed) and
b-darkening compensation. The processing also accounts for artefacts affecting many of the images, including some very speci
facts, such as bright arcs found in Kyoto and Yerkes data. Our employed methods have previously been tested and evaluated
thetic data and found to be more accurate than other methods used in the literature to treat a subset of the data analysed here.
sults. We produced a plage area time-series from each analysed dataset. We found that the differences between the plage ar
ved from individual archives are mainly due to the differences in the central wavelength and the bandpass used to acquire
at the various sites. We empirically cross-calibrated and combined the results obtained from each dataset to produce a compos
es of plage areas. The 'backbone' approach was used to bridge the series together. We have also shown that the selection of
kbone series has little effect on the final composite of the plage area. We quantified the uncertainty of determining the plage ar
our processing due to shifts in the central wavelength and found it to be less than 0.01 in fraction of the solar disc for the avera
ditions found on historical data. We also found the variable seeing conditions during the observations to slightly increase the pl
s during the activity maxima.
nclusions. We provide the most complete so far time series of plage areas based on corrected and calibrated historical and mod
II K images. Consistent plage areas are now available on 88% of all days from 1892 onwards and on 98% from 1907 onwards.

words. Sun: activity – Sun: photosphere – Sun: chromosphere – Sun: faculae, plages

duction

a need for obtaining a better understanding of long-term
gnetic activity, which is also important for studies of
's climate (Haigh 2007; Gray et al. 2010; Ermolli et al.
2013; Solanki et al. 2013). These goals require exten
reliable solar activity indices (e.g. Kopp et al. 2016; Y
2017; Shapiro et al. 2017; Wu et al. 2018).

One such dataset comes from the collection of
Ca II K observations. Numerous Ca II K archives, reco
stored at various observatories all over the world, ha
digitised over the past three decades. Presenting thei
either physical or digital form, such archives have be

---

hole series described in the paper are only available at the CDS
mous ftp to `cdsarc.u-strasbg.fr` (`130.79.128.5`) or via
`dsarc.u-strasbg.fr/viz-bin/cat/J/A+A/639/A88`

Open Access article, published by EDP Sciences, under the terms of the Creative Commons Attribution License (https://creativecommons.org/licenses/by/4.0),
which permits unrestricted use, distribution, and reproduction in any medium, provided the original work is properly cited.
Open Access funding provided by Max Planck Society.

ıs (Meftah et al. 2018; Hiremath et al. 2020), net- ll properties (e.g. Berrilli et al. 1999; Ermolli et al. 2003; ee et al. 2017; Raju 2018), photometric properties of disc over the solar cycle (e.g. Ermolli et al. 2007, 2010), as for the purpose of reconstructing of irradiance variations nolli et al. 2011; Chapman et al. 2012; Fontenla & Landi nd studies of the relation between the Ca II K bright- l the photospheric magnetic field (e.g. Loukitcheva et al. hatzistergos et al. 2019d, and references therein).

results presented in the literature on the plage area n show considerable discrepancies (Chatzistergos 2017; ergos et al. 2019b; Ermolli et al. 2018). Indeed, a criti- ct of such studies is that the accuracy of the processing to the data has not been evaluated. Also, only few indi- rchives have been used until now, and the results from archives have not been combined. This is largely because niques used for the data analysis were specifically devel- r each single archive and could not be directly applied ent data. The most employed archives are those from tri (Ermolli et al. 2009a), Kodaikanal (Chatterjee et al. Mt Wilson (Lefebvre et al. 2005), and Sacramento Peak et al. 2009) observatories.

overcome these limitations, in our previous paper tergos et al. 2018b, Paper I, hereafter) we introduced approach to process the historical and modern Ca II K tions, to perform their photometric calibration, to com- for the intensity centre-to-limb variation (CLV, here- nd to account for various artefacts. By using synthetic also showed that our method can perform the photo- alibration and account for image artefacts with higher than other methods presented in the literature. More ntly, we showed that, as long as the archives are consis- h each other, for example, they are centred at the same gth and employing the same bandwidth for the observa- e method can be used to derive accurate information on ution of plage areas without the need of any adjustments rocessing of the various archives (Chatzistergos et al. Paper II, hereafter). In Paper II, we applied our method to mages from 9 Ca II K archives to derive plage areas and the first composite of plage areas over the entire 20th In particular, we analysed the Ca II K archives from etri, Kodaikanal (8-bit digitisation), McMath-Hulbert, , Mitaka, Mt Wilson, Rome/PSPT, Schauinsland, and tein sites. Five out of the nine analysed archives were the most studied and prominent ones, while the remain- ives were from less studied data sources. There are, how- any other Ca II K archives that are available and still largely unexplored. These archives harbour the poten- ll gaps in the available plage series as well as to address tencies among the various archives and within individ- ives (e.g. change in data quality, or in the measuring ent with time). Moreover, since the work presented in , more data from various historical and modern archives available in digital form. In particular, historical data e been made available in the meantime include those e latest 16-bit digitisation of the Kodaikanal archive, Coimbra, Kenwood, Kharkiv, Kyoto, Manila, Rome, nto Peak, and Yerkes observatories, as well as additional

The paper is organised as follows. In Sect. 2, we prese data analysed in our study and the methods applied on the Our results for the plage areas from individual archives, a as the composite series are presented in Sect. 3. In Sect. discuss our results. In Sect. 5, we summarise the results study and present our conclusions.

2. Data and methods

2.1. Ca II K observations

We analysed solar full-disc Ca II K observations 43 datasets, which include series of photographic image data series acquired with CCD cameras. Table 1 summ information on the datasets analysed in our study and their characteristics. For the sake of clarity, we also list here datasets that formed the basis of the analysis and the corres ing abbreviations used in the text to refer to the various Arcetri (Ar), Baikal (Ba), Brussels (Br), Calern (CL), C (CT), Coimbra (Co), Kanzelhöhe (Ka), Kenwood (Ke), K (Kh), Kislovodsk (Ki), Kodaikanal taken with the spectr ograph (Ko), Kodaikanal taken with the Twin telescope Kodaikanal taken with the White-Light Active Region tor (WARM) telescope (KW), Kyoto (Ky), Manila (Ma), Loa (ML) taken with the Precision Solar Photometric Tele (PSPT), McMath-Hulbert (MM), Mees (MS), Meudon with the spectroheliograph (MD1), Meudon taken with an ference filter (MD2), Mitaka taken with the spectrohelio (Mi1), Mitaka taken with the Solar Flare Telescope wi interference filter (Mi2), Mt Wilson (MW), Pic du Midi SOlar Diameter Imager and Surface Mapper (SODISM) scope on board the PICARD spacecraft (PS), Rome taken the equatorial bar at Monte Mario (Ro), Rome taken wi PSPT (RP1), Rome taken with the PSPT with narrow width (RP2), Sacramento Peak (SP), San Fernando taken the Cartesian Full-Disk Telescope (CFDT) 1 (SF1), San nando taken with the CFDT2 (SF2), Schauinsland (Sc), (Te) taken with the Chromospheric Telescope (ChroTel), (UP), Valašské Meziříčí (VM), Wendelstein (WS), and (YR). Figure 1 shows examples of observations from all da except for MM and Sc, examples of which can be fou Chatzistergos et al. (2018a, 2019b). In addition to the 38 da listed in Table 1, we also analysed the five datasets includ Table 2. These five datasets include observations centred ferent locations of the wing of the Ca II K line.

The majority of the analysed datasets stem from obse ries located in Europe. However, there are datasets from As North America that provide an overall good temporal cov All in all, there are 290 147 images taken between 25/06 and 31/12/2019 covering 41 163 days. Figure 2 shows the tion of days within a year with at least one observation amo datasets considered in our study. We also show the total a coverage by the sum of all the datasets analysed here, the erage for the case when only Ko and MW are used as w for the plage area composite presented in Paper II. Fig reveals that the data analysed in our study offer a nearly plete coverage, with the exception of the period before 1944–1946, and 1986–1987. The coverage is on average for the whole period of time since 1892. However, it is on

Table 1. Ca II K datasets analysed in this study.

Observatory	Acronym	Detector	Instrument	Period	Images	SW [Å]	Pixel scale [″/pixel]	Ref.
Arcetri(a)	Ar	Plate	SHG	1931–1974	4871	0.3	2.5	1
Baikal	Ba	CCD	Filter	2004–2019	846	1.2	2.7	2
Big Bear	BB	CCD	Filter	1982–2006	5027	3.2, 1.5(b)	4.2, 2.4(c)	3
Brussels	Br	CCD	Filter	2012–2019	14699	2.7	1.0	4
Calern	CL	CCD	Filter	2011–2019	1560	7	1.0	5
Catania	CT	Plate	SHG	1908–1977	1008	–	1.1–5	6
Coimbra	Co	Plate/CCD(d)	SHG	1925–2019	19758	0.16	2.2	7
Kanzelhöhe	Ka	CCD	Filter	2010–2019	8550	3.0	1.0	8
Kenwood	Ke	Plate	SHG	1892	5	–	3.1	9
Kharkiv	Kh	Plate/CCD(e)	SHG	1952–2019	564	3.0	3.3	10
Kislovodsk	Ki	Plate/CCD(f)	SHG	1960–2019	9738	–	1.3, 2.3(f)	11
Kodaikanal(a)	Ko	Plate	SHG	1904–2007	45047	0.5	0.9	12
Kodaikanal Twin	KT	CCD	Filter	2008–2013	3059	1.2	1.2	13
Kodaikanal WARM	KW	CCD	Filter	2017–2019	585	1.0	2.4	14
Kyoto	Ky	Plate	SHG	1928–1969	3119	0.74	2.0	15
Manila	Ma	Plate	SHG	1968–1978	162	0.5	1.2	16
Mauna Loa PSPT	ML	CCD	Filter	1998–2015	31933	2.7	1.0	17
McMath-Hulbert(a)	MM	Plate	SHG	1948–1979	4932	0.1	3.1	18
Mees	MS	CCD	Filter	1982–1998	1519	1.2	5.5	19
Meudon(a)	MD1	Plate/CCD(g)	SHG	1893–2019	20117	0.15, 0.09(h)	2.2, 1.5, 1.1(i)	20
Meudon	MD2	CCD	Filter	2007–2014	1519	1.4	0.9	21
Mitaka(a)	Mi1	Plate	SHG	1917–1974	4193	0.5	0.9, 0.7(j)	22
Mitaka	Mi2	CCD	Filter	2015–2019	897	4.5	1.0	23
Mount Wilson(a)	MW	Plate	SHG	1915–1985	39545	0.2	2.9	24
Pic du Midi	PM	CCD	Filter	2007–2019	3794	2.5	1.2	25
PICARD/SODISM	PS	CCD	Filter	2010–2014	1218	7	1	26
Rome Monte Mario	Ro	Plate	Filter	1964–1979	5826	0.3	5.0	27
Rome PSPT(a)	RP1	CCD	Filter	1996–2019	3449	2.5	2.0(k)	28
Rome PSPT	RP2	CCD	Filter	2008–2019	1298	1.0	2.0(k)	28
Sacramento Peak	SP	Plate	SHG	1960–2002	7750	0.5	1.2	29
San Fernando CFDT1	SF1	CCD	Filter	1988–2015	4986	9	5.1	30
San Fernando CFDT2	SF2	CCD	Filter	1992–2013	4065	9	2.6	30
Schauinsland(a)	Sc	Plate	SHG	1958–1965	18	–	1.7, 2.6(l)	31
Teide ChroTel	Te	CCD	Filter	2009–2019	1843	0.3	1.0	32
Upice	UP	CCD	Filter	1998–2019	3234	1.6	4.0, 2.4(m)	33
Valašské Meziřičí	VM	CCD	Filter	2011–2018	318	2.4	1.8	34
Wendelstein(a)	WS	Plate	SHG	1947–1977	422	–	1.7, 2.6(l)	31
Yerkes	YR	Plate	SHG	1903–1907	7	–	2.4	35

Notes. Columns are: name of the observatory, abbreviation used in this study, type of detector, type of instrument, period of observations, total number of images (including multiple images on a single day when available) analysed in this study, spectral width of the spectrograph/filter, average pixel scale of the images, and the bibliography entry. (a)These archives were considered in Paper II, although in the case of the Ko data the earlier 8-bit digitisation was used. (b)The two values correspond to the period before and after 10/09/1996. (c)The two values correspond to the period before and after 08/11/1995, when the CCD camera was upgraded. (d)The CCD camera was installed in January 2007, but observations were stored on photographic plates up to December 2007. (e)The CCD camera was installed on 01/09/1994. (f)The CCD camera was installed on 18/12/2002. (g)The observations were stored on photographic plates up to 27/09/2002, while observations with a CCD camera started on 13/05/2002. (h)The values refer to the periods before and after 15/06/2017. (i)The values refer to the periods [24/10/1893–27/09/2002], [28/09/2002–14/06/2017], and since 15/06/2017. (j)These data derive from two digitisations and the two values correspond to the earlier and more recent digitisation, respectively. See Chatzistergos et al. (2019b) for more information. (k)The pixel scale is for the resized images to match the seeing conditions of the observing location. (l)These data were stored in TIFF and JPG files with different spatial resolution, the values correspond to the TIFF and JPG files, respectively. (m)The two values correspond to the period before and after 01/01/2018, when the CCD camera was upgraded.

References. (1) Ermolli et al. (2009a); (2) Golovko et al. (2002); (3) Naqvi et al. (2010); (4) `http://www.sidc.be/uset/`; (5) Meftah et al. (2018); (6) Zuccarello et al. (2011); (7) Garcia et al. (2011); (8) Hirtenfellner-Polanec et al. (2011); (9) Hale (1893); (10) Belkina et al. (1996); (11) Tlatov et al. (2015); (12) Priyal et al. (2014); (13) Singh & Ravindra (2012); (14) Pruthvi & Ramesh (2015); (15) Kitai et al. (2013); (16) Miller (1965); (17) Rast et al. (2008); (18) Mohler & Dodson (1968); (19) `http://kopiko.ifa.hawaii.edu/`; (20) Malherbe & Dalmasse (2019); (21) `http://bass2000.obspm.fr/data_guide.php`; (22) Hanaoka (2013); (23) Hanaoka & Solar Observatory of NAOJ (2016); (24) Lefebvre et al. (2005); (25) Koechlin et al. (2019); (26) Meftah et al. (2014); (27) Chatzistergos et al. (2019a); (28) Ermolli et al. (2007); (29) Tlatov et al. (2009); (30) Chapman et al. (1997); (31) Wöhl (2005); (32) Bethge et al. (2011); (33) Klimeš et al. (1999); (34) Lenza et al. (2014); (35) Hale & Ellerman (1903).

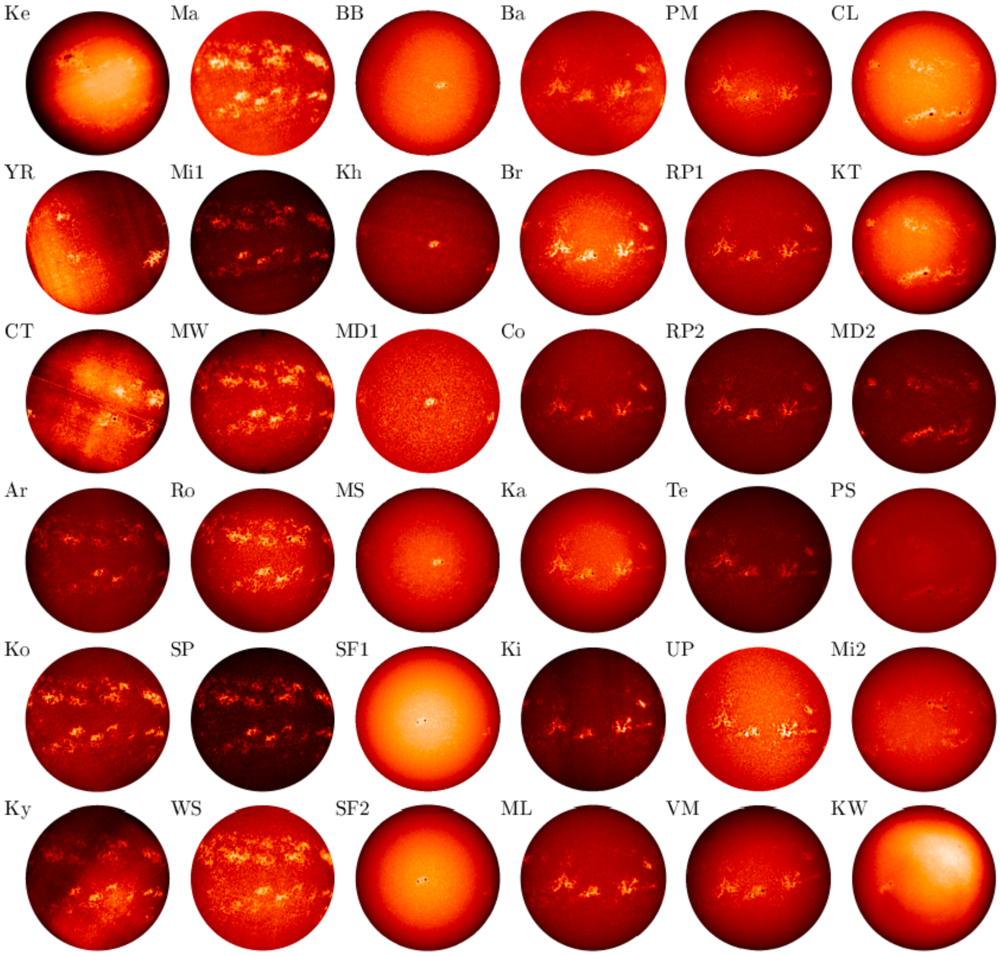

Fig. 1. Examples of observations from the various archives analysed in this study, with the exception of MM and Sc. Aside from the images in the *first and last column*, the images within each column correspond to roughly the same day. Within a column, the images are shown in alphabetical order according to the name of the observatory, given by a 2-letter abbreviation, with a numeral added in some cases (see Table 1 for the corresponding observatory name). The specific dates of the observations are: 14/07/1892 for Ke; 16/02/1907 for YR; 04/09/1908 for CT; 03/02/1968 for Ma; 04/02/1968 for Ko, Ky, Mi1, MW, and SP; 05/02/1968 for Ar, Ro, and WS; 16/07/1995 for BB, Kh, MD1, and MS; 15/07/1995 for SF1 and SF2; 13/03/2014 for Ba, Br, Co, Ka, Ki, ML, PM, RP1, RP2, Te, UP, and VM; 01/08/2012 for CL, KT, MD2, and PS; 10/07/2015 for Mi2; 23/04/2018 for KW; respectively. The images are shown after pre-processing to identify the disc and re-sample them to account for the disc's ellipticity (when applicable) and convert the historical data to density values. The images have been roughly aligned to show the Solar north pole at the top.

Ko and MW are considered is on average 80%, while it drops down to 5% in the 1990's. The composite provides full annual coverage since 2010 and for 21 more years. In contrast, the Ko and MW series together provide a full coverage only for 1967. This illustrates the substantial benefit of using multiple datasets to achieve a better coverage over the entire 20th century, but also the need to recover more historical data. The missing data from Abastumani (Khetsuriani 1981), Anacapri (Antonucci et al. 1977), Baikal, Cambridge (Moss 1942), Catania, Crimea, Ebro (Curto et al. 2016), Huairu (Suo 2020), Kandilli (Dizer 1968), Kenwood, Kharkiv, Kislovodsk, Locarno (Waldmeier 1968), Madrid (Vaquero et al. 2007), Manila, Meudon, Yerkes, Wendelstein, and Schauinsland would be invaluable for this purpose.

Tables 1 and 2 illustrate the diversity of the analysed data in terms of, for example, instruments, bandwidth used, central wavelength, and the resulting pixel scale of the images. The observations from 14 of these datasets were stored on photographic plates (we will refer to all physical photographs as plates, even though celluloid film was used by some archives), a CCD camera was exclusively used for 25 datasets, while

2. Off-band Ca II K datasets analysed in this study.

Observatory	Acronym	Instrument	Central wavelength [Å]	Period	Images	SW [Å]
Coimbra[a]	CoW	SHG	3932.3	2008–2018	3113	0.16
Mauna Loa PSPT	MLW	Filter	3936.3	2004–2015	9552	1.0
Meudon	MDV	SHG	3933.4	2002–2017	5717	0.15
Meudon	MDR	SHG	3934.0	2002–2017	5652	0.15
Meudon[a]	MDW	SHG	3932.3	2002–2018	4632	0.15

s. Columns are: name of the observatory, abbreviation used in this study, type of instrument, central wavelength, period of observatic
ber of images, and the spectral width of the spectrograph/filter. [a]Here we restricted our analysis only to the CCD-based data centred at
of the line from the CoW and MDW series. Note, however, that off-band data from these sources extend back to 1925 and 1893, respectiv

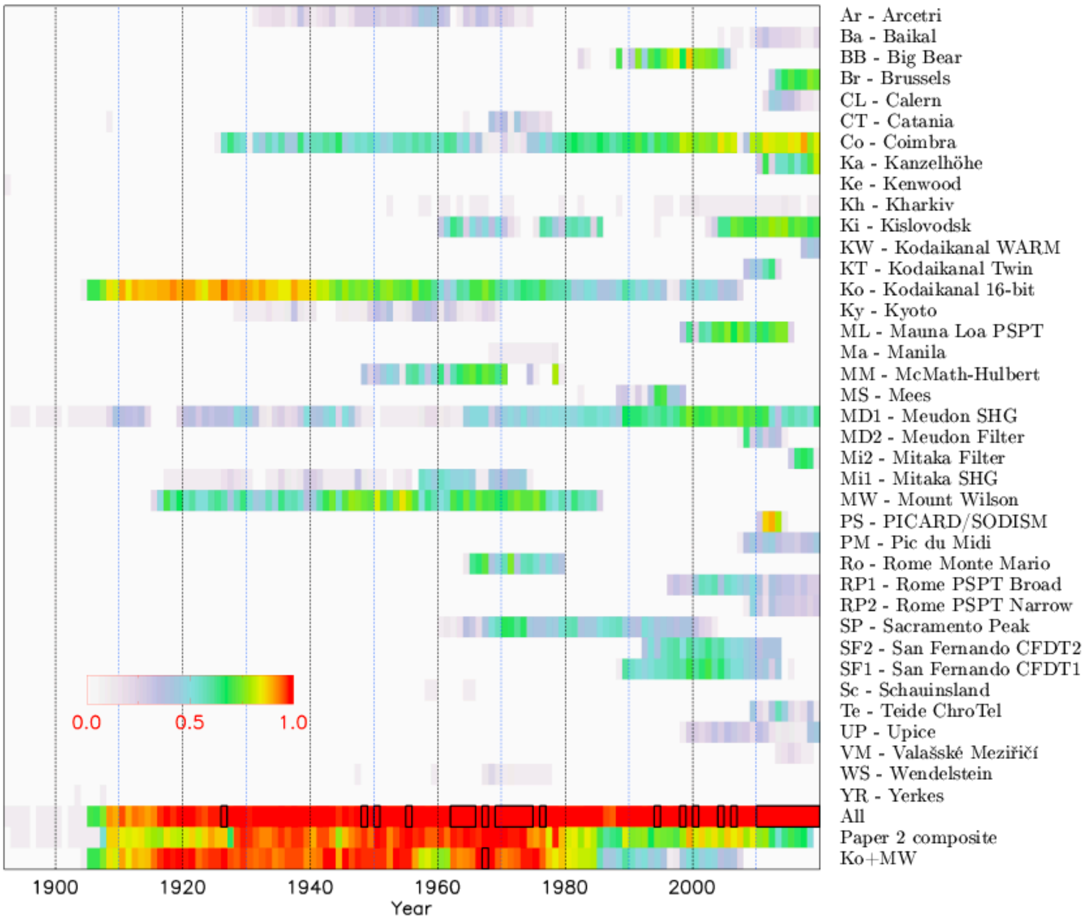

2. Annual coverage of the various Ca II K archives analysed in this study, except from those taken off-band (see Sect. 2 for details). A
n is the annual coverage of all the archives combined, the one for the Chatzistergos et al. (2019b, Paper II) composite series, and the ann
rage when only Ko and MW are considered. The annual coverage is colour-coded as shown by the colour bar plotted in the bottom left cor
e panel. Years with full coverage are outlined with black rectangles.

datasets include data taken with a CCD camera as well
tored on photographic plates. We note that a few datasets
ıde images obtained at the same observatory, but with differ-
elescopes or instruments, for example, with Kodaikanal and
aikanal Twin or Meudon spectroheliograms and Meudon fil-

tergrams. However, we do not make a distinction with reg
to the medium used to store the original data, whether it wa
CCD camera or photographic plates. We note that this catego
sation is merely to simplify the discussions in this manuscri
The arrangement of the datasets for the calibration procedu

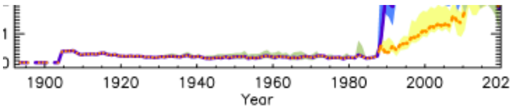

Average nominal bandwidth from all 38 archives included in this solid purple) as well as from all archives excluding SF1 and SF2 d orange). The shaded areas show the 1σ uncertainty.

duce the plage area composite is different and is out- n Appendix B. The majority of the data stored on photo- c plates were acquired with a spectroheliograph, with only cluding images taken with an interference filter. In con- that, most data taken with a CCD camera were obtained nterference filters, with only Co, MD1, Kh, and Ki images ng from a spectroheliograph. These four datasets include ken with a CCD but also stored on photographic plates. int also that Meudon data over 2002–2017 are provided a cubes with observations taken at the core of the Ca II K well as centred at four different wavelengths away from re. In our derivation of the plage area series, we included he observations taken at the core of the line (referred to as and the images taken at two extreme offsets (MDV and hereafter, for the data centred at the violet and red wing line). To discuss our results, we also analysed Meudon oimbra observations centred beyond the K1 violet wing of e (MDW and CoW, respectively), as well as Mauna Loa entred at the red wing of the line (MLW, hereafter). All the nd observations are summarised in Table 2.

e bandwidth of the analysed observations ranges between d 9 Å, thus sampling substantially different heights in the tmosphere. These differences can be seen in Fig. 1, where ages with relatively narrow bandwidth appear to have contrast in the plage regions, while the CLV is reduced red to those with broader bandwidths. In particular, the ations from MD1 and SF1 are quite indicative, having aken on the same day with nominal bandwidth of 0.15 Å, respectively. Consequently, the network regions are ced in the MD1 image, while they are barely discernible one from SF1. Conversely, sunspots are clearly visible in 1 image, but barely hinted at the MD1 one. Comparing nd RP2, taken with a bandwidth of 2.5 and 1 Å, respec- the sunspots are only minutely reduced in size in RP2, the CLV has also been reduced.

is noteworthy that modern datasets include observations in general with broader bandwidths than the ones used historical data. Figure 3 shows the annual mean value nominal bandwidth from all datasets included in this for which we have information on the bandwidth and for the observations were centred at the core of the line. It resting that there is a slight decrease in the mean band- between 1905 and 1920 while it remains roughly constant und 0.3 Å up to the late 1980's. The variations over that are rather low, with average bandwidths being in the range 5 Å. However, the variations are more extreme since 1987, range of average bandwidths between 0.4 and 3.6 Å. To degree this increase is due to the broad bandwidth of SF1

than over other periods and the bandwidths change signi the uncertainty of cross-calibrating results from Ca II over that period is also higher. However, we note that tral wavelength also affects the brightness of the magn tures in the images and consequently their disc cover also note that some datasets appear to include observatio slightly offset from the core of the Ca II K line. This for instance, the observations from ML, which have wavelength of 3934.15 Å instead of 3933.67 Å. Unfor the precise values of the central wavelength used for th vations from most archives are not available, so we able to show its change over time. Furthermore, the obse from Ka, PM, and VM have almost the same nomin width as RP1 (3.0, 2.5, 2.4, and 2.5 Å, respectively), the CLV is stronger in the Ka, PM, and VM observatio pared to the RP1 ones, hinting that Ka, PM, and VM tions might have been taken outside of the line centre o actual bandwidth is broader. A similar evaluation is m cult for the historical data, which suffer from more arte the modern data. We only mention here that SP obse taken with a nominal bandwidth of 0.5 Å, have the low among all datasets analysed in our work. This suggests actual bandwidth used at SP might be narrower than the value.

Furthermore, we note that in addition to a bandw ferent from the nominal one, there are other paramete observation that can affect the data. Indeed, paramet as stray light contribution, blurring due to atmospher over- or underexposure of photographic plates, vi instrument- and setup-specific filter transmission profile tial contamination from secondary lobes in the filter tran profile may have affected the CLV. We point out that a ern data are affected by problems. For instance, a few M taken with a CCD were found to be saturated. Finally, tions from various sites have been copied and shared w observatories. Therefore, it could also happen that ima been scanned and erroneously attributed to a wrong obs

It is also worth mentioning that some of the datase in Table 1 underwent multiple digitisations, for examp from the Ko, Mi1, MW, and SP observatories, which w tised with 8 and 16-bit devices. Compared to the ana Paper II, in this study we included 34 more datasets, as a new version of the Ko, MD1, and MW datasets. ticular, we used the Ko data from the more recent 16- tisation, MD1 data over the period 1939–1948 and 196 which had not been available before, along with recentl ered data from the MW dataset. The MW dataset stems 16-bit digitisation by Lefebvre et al. (2005), which is t as the one used in Paper II. The complete original data however, considered lost due to a failure of the stora ware. Luckily, it was recently recovered, and we foun includes 3463 images which were missing from the data sidered in Paper II. However, 164 images from the dat were considered in Paper II are still missing in the ne In this study, we analysed the recently recovered series MW data, but included the missing 164 images from th sis by Paper II. Furthermore, observations from CT, Ko, and WS were found in 35 mm celluloid films, which the same scanner previously used for the Ro observations hatzistergos et al. 2019a). The datasets from CT, Ke, Kh, Ki, a, MD1, Sc, WS, and YR have only been partially digitised. nsidering the large gaps in observations in the BB and MS tasets, it is possible that more data were taken over the 1980's, ich, however, we were so far unable to recover.

Finally, although the datasets from Ba, CL, Ka, PS, Te, and M have multiple observations per day, for our analysis we ed either the 'best' observation of the day, as selected by the servers of the BK and VM datasets, or for the CL, Ka, PS, and datasets, we used an automatic process to randomly select tween one and three images per day which were unaffected by ud coverage. We did make one exception for the first seven ys in June 2014. For this period, we analysed all available servations from all datasets to study the sensitivity of our sults to daily variations in seeing (see Sect. 4 for more details). e period was chosen randomly, with the only requirements ing that it ought to be an active period and in the summer to sure improved seeing conditions. In this way, we provide a ver estimate of the uncertainty in the derived plage areas due seeing variations. Within these seven days there are 36, 62, , 1640, 79, and 561 images in the Ba, Br, CL, Ka, ML, and Te tasets, respectively.

2. Methods

e consistently processed all images with the methods described Chatzistergos et al. (2018b, 2019b, 2020). To describe our tions in brief, we started by identifying the solar disc to extract e information on the coordinates of the disc centre and the lius (Chatzistergos et al. 2019b, 2020). We applied the cali- ation for the digitisation device, where the relevant data were ailable. In particular, the Ko, KW, and MS datasets include the propriate information to make it possible to perform the cal- ration of the CCD employed for the digitisation and observa- n, respectively. The CCD calibration has also been applied to 3 (only over the period between 07 July 2000 and 21 Septem- r 2006), Co, KT, MD2, Mi2, RP1, and RP2 data, but it has t been applied, or it is unclear whether it has been applied, the images from the other datasets. However, the flat-field ages taken at KW were found to exhibit large saturated areas, nce, we decided not to use those flat-field files. Here, we stress it the image calibration of the CCD recording device improves e accuracy of the analysed images and allows for removal of efacts due to the device and its use, for example, the dust on e detector. Figure 4 shows examples of the calibration of the D recording device for Ko, MS, and RP1 images. All the libration data shown here exhibit intensity variations across e different quadrants of the CCD. Additionally, numerous dark all-scale round artefacts are evident in the MS observation. e flat image for the Ko observation also shows some scratch- e patterns. Such artefacts are accounted for by using the cal- ration images, thus reducing the uncertainties of analysing ese data. Besides, for all datasets we applied a data selection hatzistergos et al. 2019b) merely to exclude pathological cases aracterised by severely distorted discs, missing parts of the c, or strong artefacts over the disc. Moreover, the solar disc in 3, Co, Kh, Ki, MD1, MW, SP, and Te images was re-sampled account for its ellipticity following Chatzistergos et al. (2020).

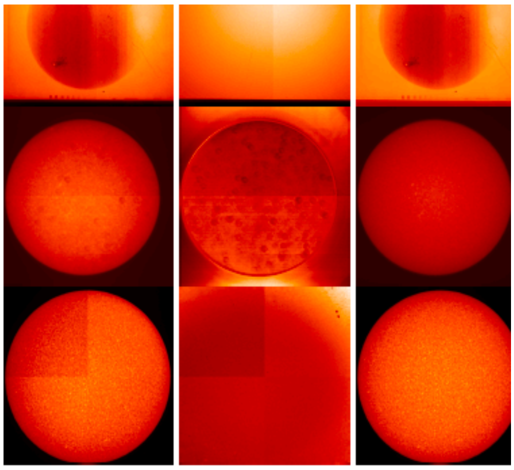

Fig. 4. Examples of raw images (*left column*), data employed f calibration of the CCD recording device (*middle column*), and brated images (*right panels*) from the Ko (*first row*), MS (*middle* and RP1 (*bottom row*) archives taken on 19/08/2006, 19/12/199 28/02/2020, respectively. The images have not been compensat ephemeris and are shown in their entire range of values.

et al. 2018b) to account for the non-linear response of the p graphic material. All images, historical and modern, were pensated for the limb-darkening as described in Paper I. Ir ticular, we define a contrast image as $C_i = (I_i - I_i^{\rm QS})/I_i^{\rm QS}$, v C_i, I_i are the contrast and intensity values of the calibrated i at pixel i, while $I_i^{\rm QS}$ is the intensity of the quiet Sun (QS, after) at the pixel i. Ky and YR data suffer from a very sp artefact manifesting itself as bright or dark arcs on the disc. Therefore, to improve the accuracy of the analysis c Ky and YR data we added one further processing step. The cess applied on these data is described in detail in Append Figure 5 displays examples of the calibrated and limb-dark compensated contrast images after the preprocessing to cc for the elliptical discs (where needed) and to convert the hi cal images to density values for the same observations as sl in Fig. 1. More details on: the processing of the Ar, MM, M Mi1, MW, RP1, Sc, and WS datasets can be found in Pap on processing the CT and Ro datasets in Chatzistergos (2019a); Ko in Chatzistergos et al. (2019c); and Ky and Chatzistergos et al. (2020).

All the processed images were segmented to identify areas with a multiplicative factor, $m_p = 8.5$, to the star deviation of the QS regions (Chatzistergos et al. 2019b). segmentation was applied consistently with the same r plicative factor to all the datasets. The observation time f archives was converted to Universal standard time (UT). Fig shows the corresponding segmentation masks of the obs tions shown in Fig. 1, singling out the plage regions, whic the solar features that are mainly considered in this study.

3. Analysis of the Ca II K series

3.1. Individual Ca II K series

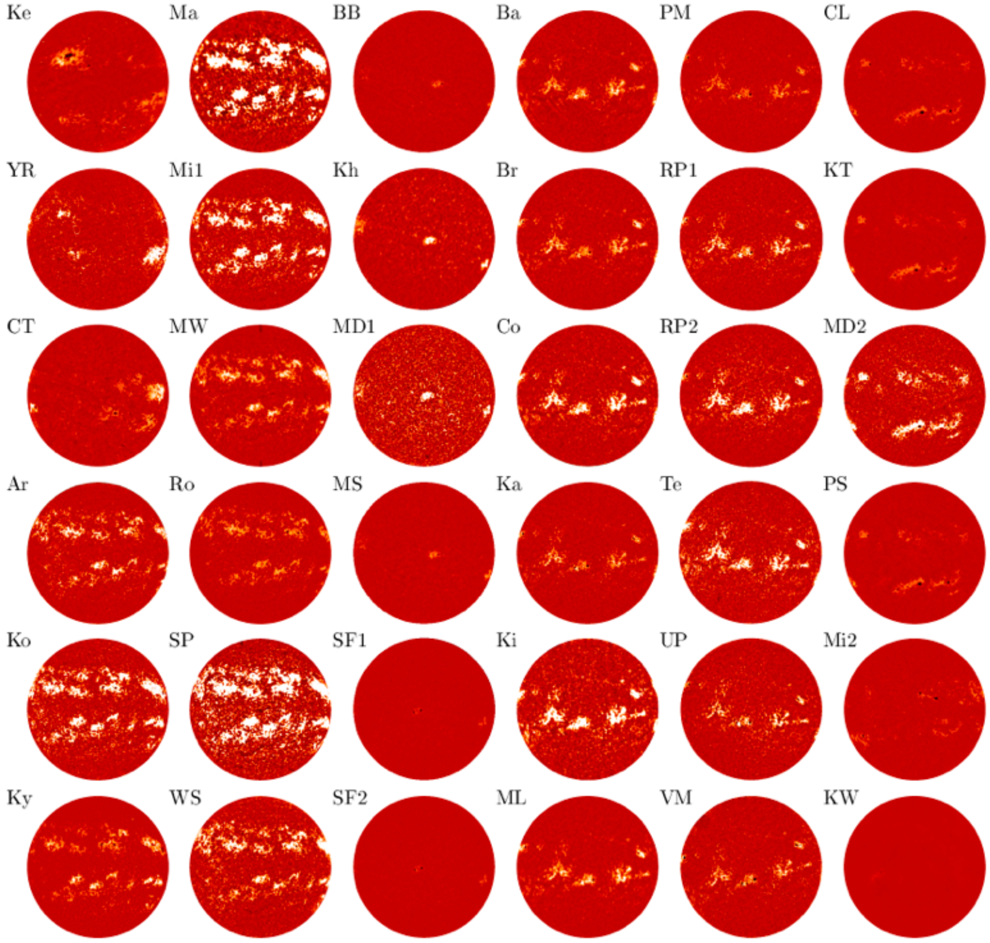

Fig. 5. Calibrated and CLV-compensated contrast images of the observations shown in Fig. 1. Plotted are contrast values in the fixed range of [−0.5,0.5] for all images.

panels, each one showing periods of roughly four solar cycles (SC). The temporal profile of the evolution of plage areas is, in general, similar. Thus, we can recognise the same features in all datasets during various periods; for example, the period 1971–1975 or the double peaks of SC 22 maximum over the period 1989–1992. However, there are also some obvious differences.

For instance, the plage areas from Ka, KW, Mi2, PM, UP, and VM are considerably lower than those of all other datasets. This is in agreement with the comment in Sect. 2 that these data were probably taken off-band or with a broader bandwidth. The plage areas from Co are considerably lower than from other datasets over SC 20. However, the annual values from Co data are not representative over that period due to the low number of Co images because of the relocation of the observatory (Lourenço et al. 2019). We also note that the Co plage areas over SC 19 are lower than SC 17 and 18, hinting at a potential issue with the data over SC 19. Plage areas derived from Kh images are greater than those from Ko data over SC 23. This is contrary to the expectation considering that the bandwidth used at Kh is double the one used at Ko. Given that both observatories employed spectroheliographs[1], this lends support to our suggestion that the actual bandwidth of the Ko observations is broader than reported or there is an offset in the central wavelength (Chatzistergos et al. 2019b,c).

We also compare the SF1 and SF2 series. These data have the same nominal observational characteristics except for the spatial resolution, which in SF1 data, is half of that in SF2 data. We find a linear correlation factor of 0.9 and RMS differences of 0.005 between the determined plage areas of the two series when considering only the 3821 days for which observations with both telescopes exist. These differences are at least partly due to the

---

[1] We remind that Kh used a CCD camera after 1994, while Ko used only photographic plates.

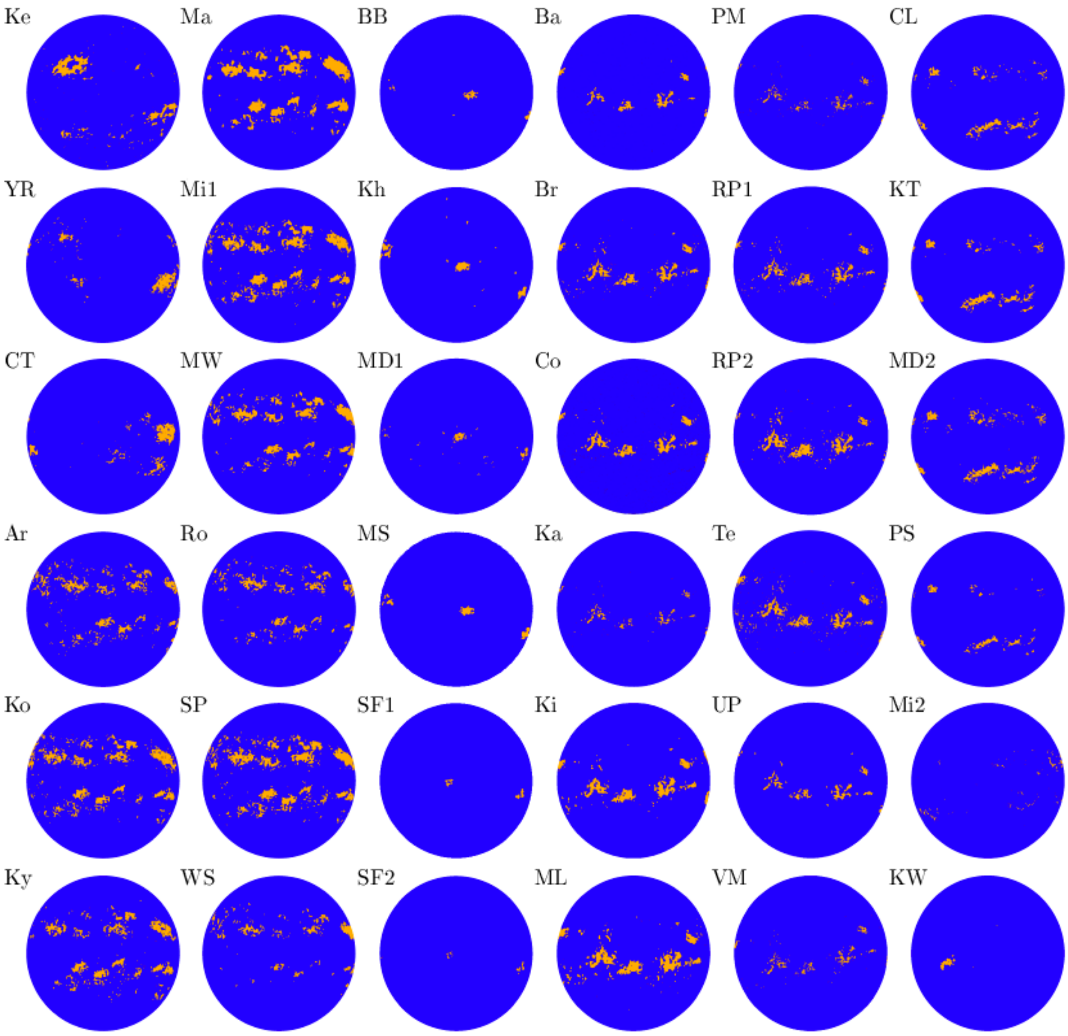

ig. 6. Segmentation masks derived from the observations shown in Figs. 1 and 5. Plage are highlighted in yellow, while quiet Sun and netwo gions together form the blue background. We note that the same threshold was used for all datasets to identify the plage regions, which is wh e different datasets seem to give rather different plage coverage depending on the employed bandwidth or central wavelength.

wer resolution of SF1 data compared to the SF2 ones, which sults in some smearing of the features. However, this discrepcy might also be due to potential issues with SF1 data during 97–2001. This is evidenced by a sharp increase of plage areas er 1997 and a decrease between 2000–2001, around the activy maximum of SC 23. When excluding the data between July 97 and December 2001 we find a linear correlation factor of 95 and RMS differences of 0.003.

2. Plage areas composite

Paper II, we presented a plage area composite derived from e analysis of nine Ca II K archives. The composite of plage eas was the average series of those obtained from using the sults from the eight-bit Ko and 16-bit MW series as the ferences. In this study, we present a plage area composite obtained on the basis of the results from 38 datasets. Thes include the data from the 16-bit digitisation of the Ko datas (Chatzistergos et al. 2019c) as well as the recently recovered da from the 16-bit digitisation of MW. Furthermore, we use a di ferent methodology to create our plage area composite serie employing the "backbone" approach (Svalgaard & Schatte 2016; Chatzistergos et al. 2017). In particular, we split th datasets into two backbones, roughly representing the histor cal and modern data separately. We took the RP1 series as th reference for the modern data backbone, while we used the K and MW series as references for the historical data. Appendix describes the assignment of the various analysed series to th backbones.

Following Paper II, we cross-calibrated the individual serie to the ones entering the backbone by using the daily stati tics of the determined plage areas. In particular, we starte

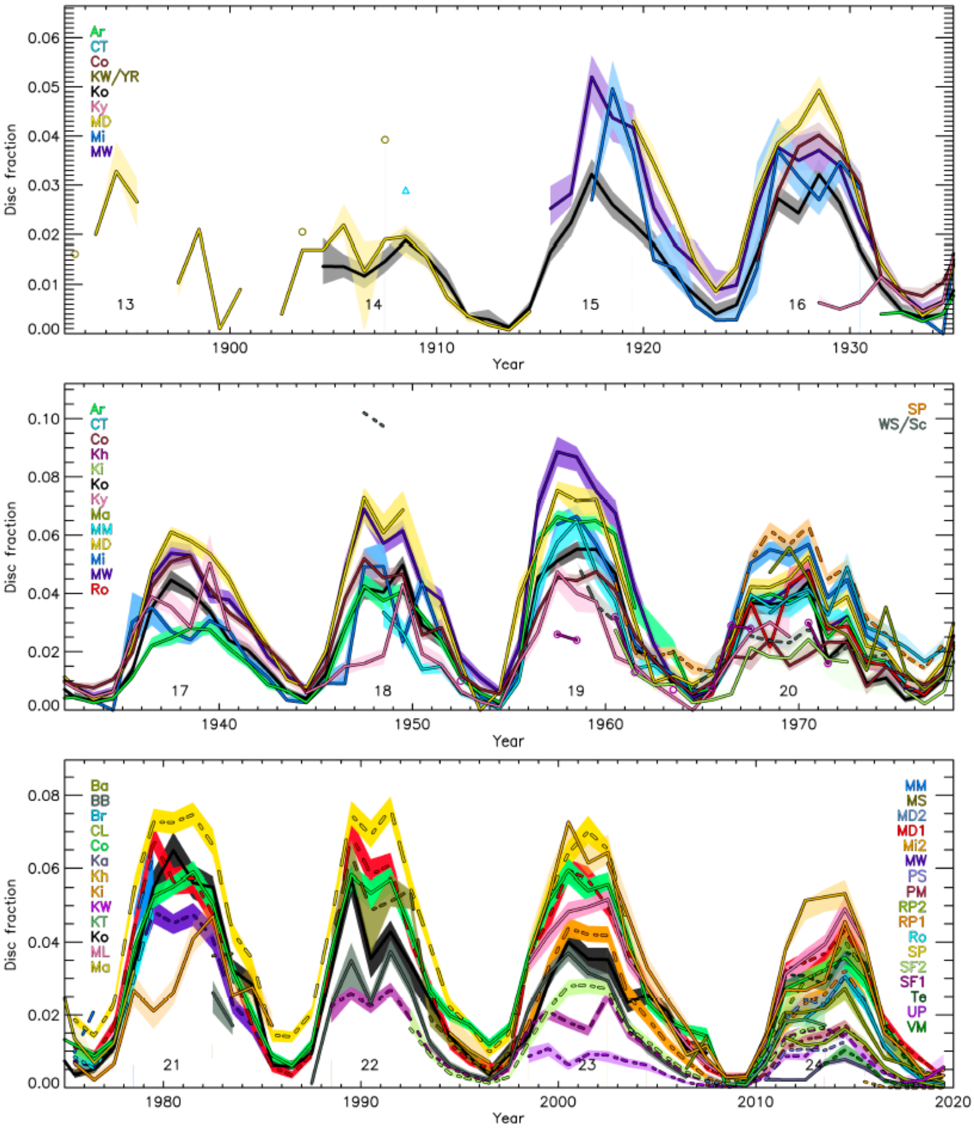

Fig. 7. Evolution of plage areas given as fraction of the solar disc derived from analysis of the 38 datasets considered in this study. Shown are annual median values (lines) along with the asymmetric 1σ interval (shaded surfaces) for each dataset as specified in the legend. To improve visibility, the archives listed in the legend in the right side of the plot are represented by dashed lines. Due to the scarcity of observations, the plage areas derived from the Ke/YR and CT observations in the top panel, as well as the Kh in the middle panel are represented by circles, triangles, and circles, respectively. The conventional solar cycle (SC) numbers are given below the curves.

by computing daily mean plage areas for all series. Then, we constructed a probability distribution function (PDF, hereafter) matrix between each individual series and the corresponding backbone one. To create this matrix we first identified the days for which both series have a plage area measurement. Then we separated these days into arrays for which the secondary series reported plage areas in bins of 0.001 in disc fraction. For each of these arrays, we computed the histogram of the reported plage areas from the backbone series in bins of 0.001 in disc fraction. For each of those selected arrays, we normalised the histogram with the total number of data within that array, thus creating a PDF. See Chatzistergos et al. (2017) or Paper II for

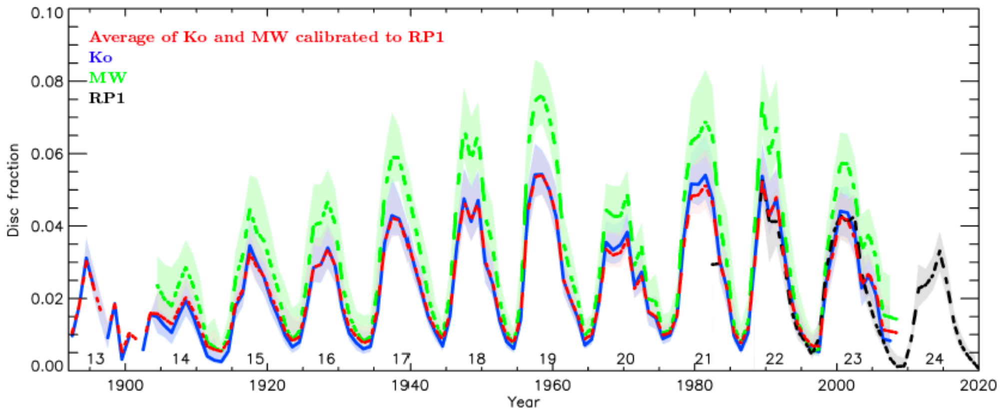

Fig. 8. Backbone series of plage areas by using as reference the series from RP1 (dashed black), Ko (solid blue), MW (dashed green), and the average backbone of the MW and Ko series after their cross-calibration to the RP1 one (dashed red). Shown are annual median values (lines) along with the asymmetric 1σ interval (shaded surfaces). The solar cycle numbers are given below the curves.

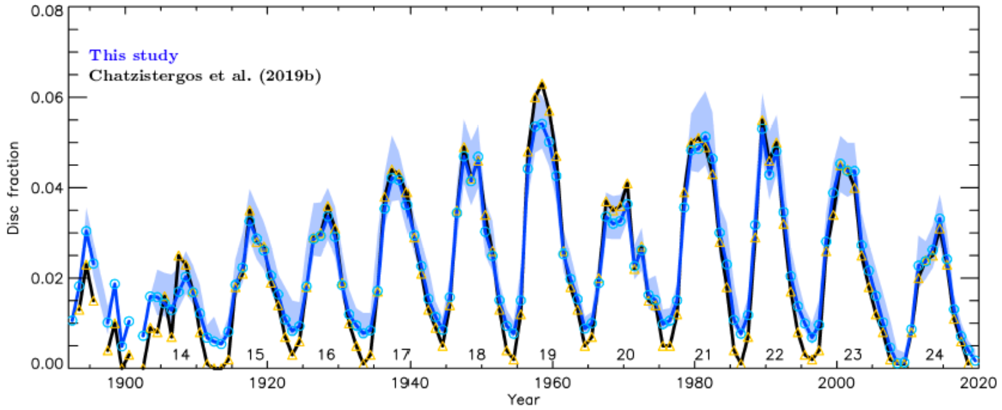

Fig. 9. Composite of plage areas in disc fraction derived in this study (blue line and ciel circles) along with the composite by Chatzistergos et al. (2019b, black line and yellow triangles). Shown are annual median values (solid lines and symbols) along with the asymmetric 1σ interval (shaded surfaces). The solar cycle numbers are given below the curves.

more details on this process. We computed the mean value of each PDF along with the asymmetric 1σ interval, which we used to perform a weighted fit of a power law function with an offset (Chatzistergos et al. 2019b) and a linear fit. These relationships were used to scale the plage areas of the secondary series to the level of the backbone one. Following Paper II, we used the linear relation for the Ko and RP1 backbones, while we used the power law for the MW ones. All calibrated series were appended to the backbone one to create the backbone composite series. This way we construct one backbone for the modern data and two for the historical ones. We cross-calibrated the two historical backbone series and the RP1 backbone series in the same way as done for the individual series. Then the two historical backbone series were averaged to create the average historical backbone series.

Figure 8 shows the RP1, Ko, MW, and the average historical backbone. We note that the Ko and RP1 backbones are at similar levels over SCs 22 and 23, with the latter being slightly lower. The variation of the plage areas in the MW backbone has higher amplitude than in the other backbone series by ~0.15 in disc fraction. The average historical backbone (average backbone series of Ko and MW after their cross-calibration to RP1) appears very similar to the raw Ko backbone, with most SCs after SC 20 being slightly reduced in amplitude. We note that over SC 23 the plage areas in all backbone series except the RP1 exhibit a secondary peak around 2004. This is attributed to the Ko data over that period as was also mentioned by Chatzistergos et al. (2019c).

Figure 9 shows the final composite[2] produced by merging the RP1 and the average historical backbones as well as the plage area composite obtained in Paper II for comparison. The two composites agree on the absolute level, which is expected since in this study we used RP1 as the reference, while the composite presented in Paper II had a scaling factor of 1 for RP1. However,

---

[2] Available at `http://www2.mps.mpg.de/projects/sun-climate/data.html`

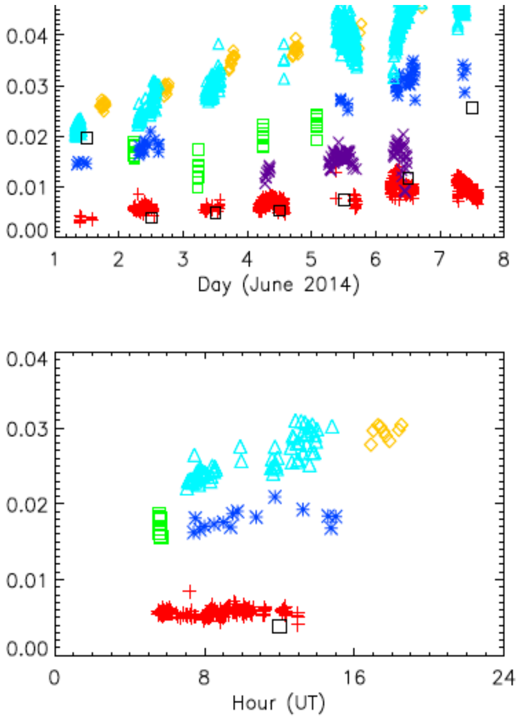

). Plage areas in disc fraction as a function of time from the s of Ba (green squares), Br (blue asterisks), CL (purple x sym-nly in the *top panel*), Ka (red plus signs), ML (orange rhom- and Te (ciel triangles). Results are shown for individual images e course of the first week in June 2014 (*top panel*) and over the of 02 June 2014 (*bottom panel*). Also shown are the sunspot y Balmaceda et al. (2009, black squares) multiplied by ten to hem to roughly the same level as the plage areas for the sake of rison.

ice that the plage areas at the maxima of SC 14, 19, 20, 22, are slightly reduced in the new composite with respect to in Paper II, while most minima are slightly elevated. The se of the values over activity minima is partly due to the ion of more data taken with a relatively narrow bandwidth ired to the composite in Paper II. Similarly, over SC 19, wly added data favour lower activity level compared to MW or MD1 data. However, we note that the majority 1 data over SC 19 are still not digitised, which may affect mposite series.

scussion

ve focus on the uncertainties of our results due to charac-s of the analysed data, that is, the relevant seeing condi-or central wavelength used for the observations, as well as due to our method of producing the composite plage area The accuracy of the methods applied to the processing of servations was tested and discussed by Chatzistergos et al. , 2019b,c).

st, we estimate the sensitivity of daily plage areas analysed all available observations of the first week of 2014. Figure 10 shows the derived plage areas over that pe Over those days, the plage areas from all datasets as well a sunspot areas show a roughly steady increase. We also n the derived plage areas to increase through the course of day, which is consistent with the worsening seeing condit towards local noon, that smears the plage regions. Howeve least part of this increase is due to the increase of solar a ity over the course of that week. This increase is expecte be greater for the archives with observations taken with na bandwidths, such as Te. We find the areas from Ka to show stable values within a given day, with only a slight increa the areas around 06:00 UTC followed by a slight decrease that. The results in Fig. 10 allow a rough estimate of the u tainty of the derived plage areas due to the seeing condit during the acquisition of the images. We find the areas fro Br, and CL observations to exhibit a typical daily variati ~0.01 in disc fraction, with a somewhat lower variation f and Ka data (about 0.005), and a greater variation (up to a 0.02) for ML data. We cannot judge whether the bandwid the observations has any effect on these results.

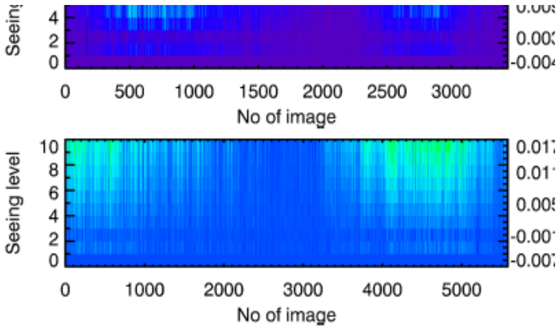

Fig. 11. Colour-coded difference in fractional plage areas derived RP1 (*top*) and MD1 (*bottom*) images downgraded to simulate e of seeing and those derived from the original RP1 and MD1 im respectively. The MD1 data used here are only those taken w CCD camera between 2002 and 2017. Each row (column) of shows results derived from a given observation (width of the smoo Gaussian function). See Sect. 4 for details.

However, the passage of plage regions over the disc, pa which can go behind the limb or appearance of new plage reg at the limb within a day, also affects these results. To remove uncertainty, we also simulated the effects of seeing on RP1 MD1 images by applying on them a Gaussian smoothing with varying widths. We used ten values for the width unifo distributed in the range [0,2] σ, where σ is the standard de tion of the Gaussian function. Figure 11 shows the residual fractional areas derived from the smoothed and the original smoothed) images. Similarly to the results of the actual arch we find a variation in the plage areas with generally higher v for the smoothed images. This might come as a surprise co ering that the plage areas are smoothed and hence their area expected to get reduced. However, the smoothing also decre the standard deviation of the QS regions, hence our thresho isolate the plage areas is lower compared to the original im

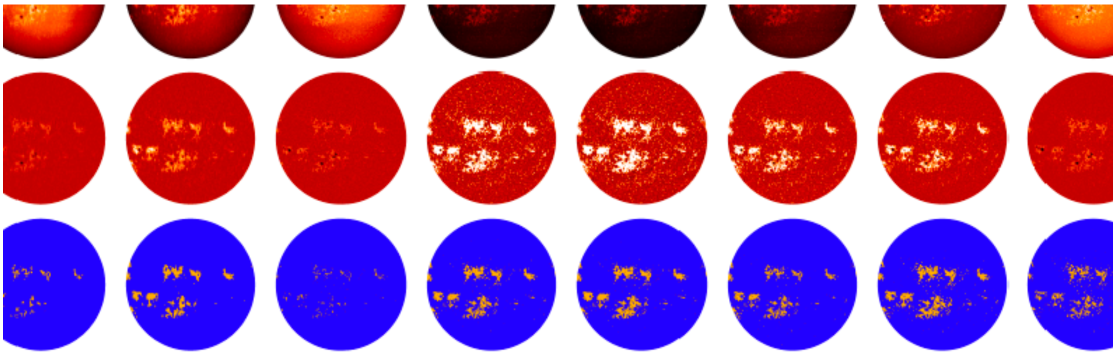

. Examples of observations taken on the same date (04 July 2014) from the various datasets analysed in this study with images no
ore of the Ca II K line along with those from the same observatories centred at the core of the Ca II K line. Shown are images f
o, MDW, MDV, MD1, MDR, ML, MLW datasets after the preprocessing to identify the disc and re-sample them to account for
ty (*top row*), after CLV-compensation (*middle row*), and after the identification of plage (*bottom row*). The images have been al
e solar north pole at the top. The raw images are shown to their entire range of values, the CLV-compensated images are show
-0.5,0.5], while in the masks, the plage regions are shown in orange and the quiet Sun and network regions in blue. We stress that t
ld was used for all datasets to identify the plage regions, which is why the different datasets seem to provide rather different ranges
e.

sults for the MD1 and RP1 data are almost identical. The fferences we identified are that MD1 data have marginally errors (up to 0.017 instead of 0.019 found in RP1 results considering the common observations to MD1) and that re images for which the plage areas decrease slightly more P1 ones (minimum value of −0.007 instead of −0.002 in RP1 data for the common days to MD1). The values for ferences in the plage areas are consistent with the results actual datasets.

also estimate the uncertainties in the derived plage areas variations in the central wavelength of the observa- All Ca II images can exhibit such variations, irrespec- of whether they were taken with a spectroheliograph, or interference filter. In the case of the spectroheliograph, iations are due to the positioning of the slit, for exam- cause the observers intentionally or unintentionally took ations off-centred from the line core. In general, cases the observers intentionally took observations off-centred umented, as in the archives from MD1 and Co for which ations centred at K1 and K3 are separated (the former are d MDW and CoW, respectively, in this paper, while the re abbreviated as MD1 and Co). However, this practice t always documented consistently for all of the datasets red in our study. In the case of the interference filters, the ons are more consistent and mostly due to the replacement filters or filter degradations, manifesting as a single offset ift in time, respectively.

order to test the effects of the different central wavelength derived plage areas we used the off-band observations oimbra, Meudon, and Mauna Loa. Meudon has observa- ver the period 2002–2017 taken at four different wave- around the core of the Ca II K line along with the data t the core of the line. All of those observations were taken e same bandwidth. Here we use only those taken at the of the line and the two extreme cases which correspond to

respectively. Coimbra and Meudon also have observatio tred beyond the K1V minimum, with an offset of −1.4 Å Ca II K line (CoW and MDW, hereafter), taken with th bandwidth as those centred at the core of the line. The Loa dataset includes data taken at the core of the Ca II K well as data taken 2.6 Å offset to the red wing (MLW, he of the line with a narrower bandwidth of 1 Å compared t taken at the core of the line (which have a bandwidth of

Figure 12 shows examples of these data for obse taken on 4 July 2014. We notice that the contrast of plag decreases for all data taken off-centred, and unsurpris is lower for data taken further away from the core of t Moreover, the network regions are diminished in contr the sunspots are enlarged. The MLW images are quite si the CoW and MDW ones, even though MLW is suppose taken further away from the core of the line than the oth However, the contrast of the MLW images is slightly grea those from CoW and MDW. This might be an effect of th ences in the bandwidth of these observations, with the o for MLW being considerably broader than those used f and MDW.

Figure 13 gives the absolute difference in the derive areas between the datasets centred at the core of the l those taken off-centred. The same segmentation meth applied to all the data. The plage areas derived fro datasets also decreases compared to the values we get data centred at the core of the line. The difference for t MLW data is lower than for the MD1-MDW or Co-Co reaching a value of 0.02 during activity maximum. The ences show variations following the SC, but a small also noticed during activity minimum, being on average 0.001 and 0.002 for MD1-MDV and MD1-MDW, respe The differences are greatest for the cases MD1-MDW CoW reaching values of 0.04 during activity maxima. We the typical variations of the central wavelength in the

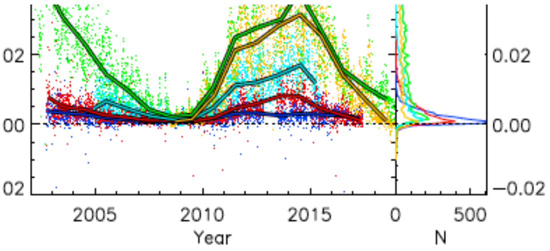

. *Left*: difference of fractional plage area between those derived
entred and off-centred Ca II K observations as a function of
he differences shown are for the Co-CoW (orange), MD1-MDW
, MD1-MDV (blue), MD1-MDR (red), ML-MLW (ciel). Dots
aily values, while the solid lines show annual median values.
tted horizontal line denotes a difference of 0. *Right*: distributions
lifferences.

ainty level in the determined plage areas from the histori- a due to shifts in the central wavelength. For MD1-MDR D1-MDV, we notice that the distribution of the differences uite narrow when compared to the other cases tested here. fferences in the derived plage areas for these cases are on e (RMS difference) less than 0.003 (0.003). However, we tice that even though the wavelength offsets for MDR and are equal in absolute value, the results for the plage areas t exactly the same. The difference in the plage areas for are greater than for MDV. This is unsurprising consider- e similarity of MDV and MD1 images compared to the ones (see Fig. 12).

xt, we tested to which degree the composite series is d by our choice of individual backbone datasets. In this s, we used all historical datasets with sufficiently long s to act as backbone references. These are the Ar, Ko, D1, MM, MW, Ro, and SP datasets. Figure 14 shows the ng plage area composite series. We did not consider Co, r Mi2 in this test due to the poor overlap with many of her datasets. Table B.1 lists the assignment of the vari- ge series to the individual backbones. For consistency, all are normalized to the level of the RP1 backbone. All pro- composites agree almost perfectly over SCs 22–24, owing RP1 backbone. However, there are disagreements for the ing cycles. The differences are greatest for the composites l with MM, Ky, and SP as the backbones for the histori- a. This is consistent with the rather low amount of data those datasets, rendering the calibration of the various non-backbone) datasets to their level more uncertain. The ing reconstructions show results that are very similar to posed series. The differences are typically below 0.005, rease over SC 19 to 0.02 for daily values. This gives a estimate of the uncertainty in our official composite series the selection of individual datasets to act as the reference. te, however, that the overlap between most of the series s backbones for this test is not optimum and is always compared to that of the Ko and MW series. Furthermore, raging the Ko and MW backbone series we reduce the ainty due to the choice of the reference series.

gure 15a shows the composite based on using RP1 as a

are considered (red). In this case the differences are lo with an RMS difference of 0.001 and a maximum differ 1999 of 0.003 in disc fraction. This illustrates the accurate calibration of the individual series to the RP1 backbone.

Finally, we also test the effect of including data take different bandwidths in the backbone series. For this purp use the RP1 backbone and produce three different versio (i) keeping only datasets with either bandwidths narrow 2 Å or broader than 3 Å (Ba, CL, Co, Kh, PS, RP2, SF Te, Up). Since the RP1 bandwidth is 2.5 Å, these limits that the chosen bandwidths differ by at least ±0.5 Å fro of RP1. (ii) including only datasets with the nominal ban between 2 Å and 3 Å, that is, within ±0.5 Å of the bandw RP1. In this case, we further subdivide the datasets acc to whether the bandwidths that have been assigned to t (a) appear to be consistent with their actual behaviour (I ML) ii (b) or their assigned bandwidth does not appear to l sistent with their actual behaviour (Ka, PM, VM). For th we considered the BB and ML datasets only over the p when the final instrumentation was used (see Append in order to avoid inconsistencies due to instrumental cl Figure 15b displays the three test backbone series in comp to the one used in our composite. All three reconstruction RP1 backbone series lie within the uncertainties. There a erally small differences, which are greater in 2011, before and after 2018, reaching up to 0.01 in disc fraction.

5. Summary and conclusions

We processed 43 datasets of full-disc Ca II K observation ning the period 1892–2019 to derive the evolution of plag over the last 12 solar cycles. We processed the data tently with the method developed by Chatzistergos et al. (2019b). An extra step in the processing was added to accurate results from the analysis of images from the Ky a datasets, which suffer from specific artefacts along arcs solar disc. We adapted our processing such that these a can be precisely accounted for and showed that we can accurate results for those datasets as well.

We used our results for the 38 datasets with observatio tred at the Ca II K line to create a plage area composite by ing the backbone approach employed by Chatzistergos (2017) to create a sunspot group number composite. We two backbones, one mostly for the modern CCD-based d another for the historical data, which were mainly stored o tographic plates. We considered the plage area series from (RP1) observations as the overall reference series and to the backbone for the modern data, while both Kodaikan and Mt Wilson (MW) acted as the references for the his data. The obtained composite on the whole reasonably sistent with the one we presented in Paper II, althoug differences exist. The composite derived in this study average annual coverage of 98% for the periods after 190 observations for only 672 days missing. The coverage, ho remains rather low for the period 1892–1906 with 491 without any observations recorded. Previous results in erature were based on considerably poorer temporal cov

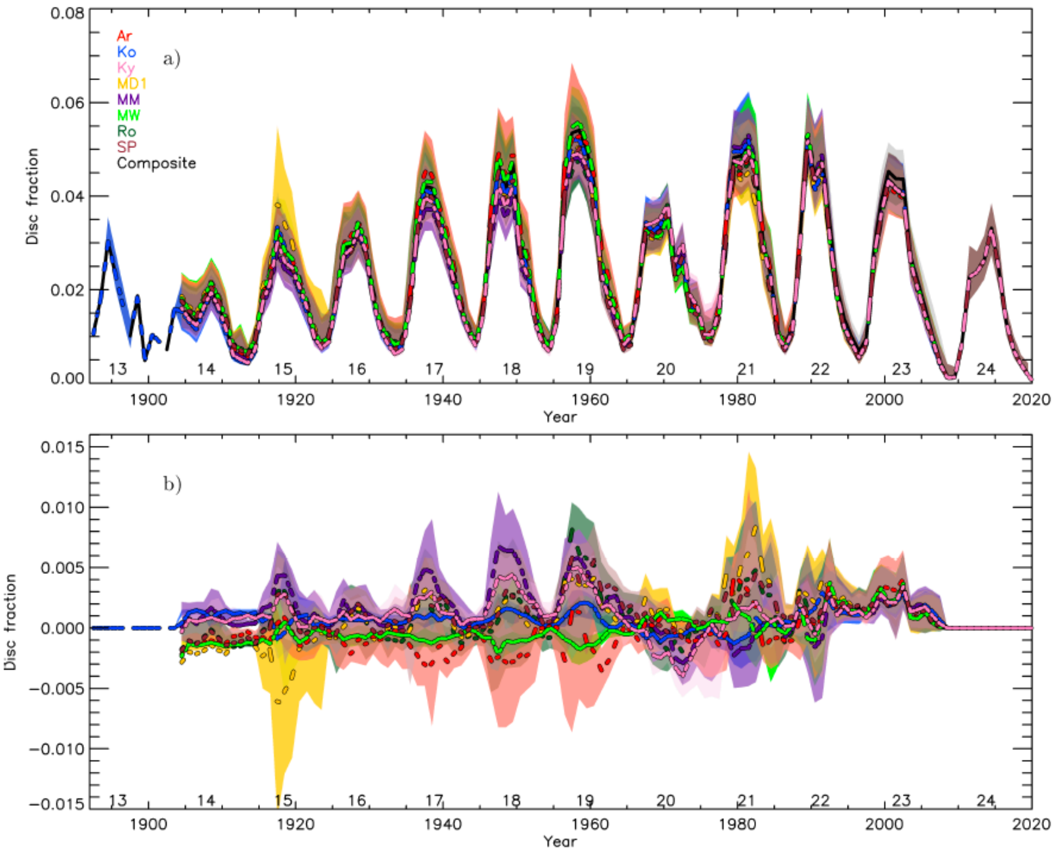

Fig. 14. Plage area composites *(a)* and their differences in comparison to our main composite series *(b)* produced when the historical backbone series was computed with various individual historical datasets as the backbone reference instead of using the average of the calibrated Ko and MW ones to the RP1 one. RP1 is always taken as the overall reference for all composite series. The datasets used as backbones are those from Ar (red), Ko (blue), Ky (pink), MD1 (orange), MM (purple), MW (green), Ro (dark green), and SP (brown) sites. The composite plage area series derived in this study is also displayed in black. Shown are the annual median values (lines) of the final plage area composites along with the asymmetric 1σ interval (shaded surfaces). The numbers below the curves denote the conventional SC numbering.

alone, which are the ones most employed in studies of the plage areas evolution so far.

Many observatories, whose data have been analysed here, have stopped the solar monitoring in the Ca II K line. However, observations in the Ca II K line continue at the Ba, Br, CL, Co, Ka, Kh, Ki, KW, MD1, Mi2, PM, RP1, RP2, SF1, SF2, Te, UP, and VM sites to this day. A combination of the data from all those sites provides a full annual coverage. There is no day without an observation in our composite series since 2010. However, there are still gaps in our composite. Hopefully, more historical archives, such as those from Abastumani (Khetsuriani 1981), Anacapri (Antonucci et al. 1977), Cambridge (Moss 1942), Crimea, Ebro (Curto et al. 2016), Huairu (Suo 2020), Kandilli (Dizer 1968), Locarno (Waldmeier 1968), Madrid (Vaquero et al. 2007), and the remaining data from the Baikal, Catania, Kenwood, Kharkiv, Kislovodsk, Manila, Meudon, Yerkes, Wendelstein, and Schauinsland sites will be digitised in the near future, which can potentially further increase the daily coverage of the data entering our composite series.

In this paper, we have aimed to shed light on various issues affecting individual Ca II K archives. We accounted for some of these in a simple manner by splitting the series into different parts and performing their cross-calibration to the backbone series separately. However, there are more issues that remain unaccounted for in our analysis, such as the variable bandwidth and central wavelength of the observations taken with a spectroheliograph. For these, we present an estimate of the uncertainty in our results. However, we plan to further address the effects due to variable bandwidth and central wavelength of the observations with a machine learning approach, considering that such methods have shown great potential on image-to-image conversion (e.g. Kim et al. 2019; Galvez et al. 2019; Park et al. 2019). In addition, we plan to continue processing the data from the currently operating programs in the Ca II K line to update the

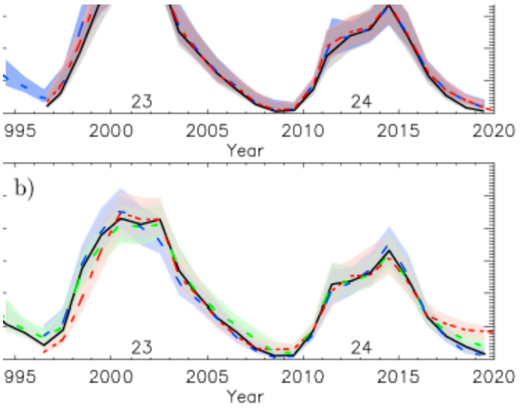

op: RP1 plage area series (solid black) plotted along with ackbone composite series used in our plage area composite lue) and RP1 backbone composite series keeping only the mon with the RP1 individual series (dashed red). *Bottom*: bone composite series when varying the included individual ased on their bandwidth. The different curves show the RP1 composite by keeping Ba, Co, Kh, RP2, SF1, SF2, Te, Up reen), Br, ML, BB (dashed blue) and Ka, PM, VM (dashed RP1 backbone series used for our composite is shown in solid picted are annual median values (solid lines) along with the netric intervals (shaded surfaces). The SC numbers are given curves.

te at regular intervals. Finally, we plan to continue g and updating the composite by including further historical ta whenever these are digitized and made available.

gements. The authors thank the observers at the Arcetri, Bear, Brussels, Calern, Catania, Coimbra, Kanzelhöhe, Kharkiv, Kislovodsk, Kodaikanal, Kyoto, Manila, Mauna Loa, McMath-lees, Meudon, Mitaka, Mt Wilson, Pic du Midi, Rome, Sacramento Fernando, Schauinsland, Teide, Upice, Valašské Meziřičí, n, and Yerkes sites for all their work in carrying out the observing We thank Isabelle Buale for all her efforts to digitise the Meudon e thank Jeff Kuhn and Cindy Maui for locating and sharing with us a II K data. We thank Satoru Ueno and Reizaburo Kitai for providing observations. We thank the anonymous referee for the constructive that improved this manuscript. We thank Ester Antonucci, Alexi gie Cookson, Martina Exnerová, Bernhard Fleck, Detlef Groote, echlin, Libor Lenža, Mustapha Meftah, Werner Pötzi, Roger Ulrich, k, and Hubertus Wöhl for providing information about various ata. This work was supported by FP7 SOLID, and by the BK21 am through the National Research Foundation (NRF) funded by y of Education of Korea. This research has received funding from an Union's Horizon 2020 research and innovation program under ment No 824135 (SOLARNET). The Coimbra researchers thank ReNATURE (CENTRO–01–0145–FEDER–000007–BPD16). We ge the "Observateurs associés" for their commitment to image acquiprocessing; IRAP for the instrumental and database management; de Toulouse, CNRS, and Fiducial for the funding. We acknowledge rvatory for the use of spectroheliograms and the Royal Observatory n, Brussels for USET data. The Kanzelhöhe Ca II K data were y the Kanzelhöhe Observatory, University of Graz, Austria. ChroTel by the Kiepenheuer-Institute for Solar Physics in Freiburg, Germany, ish Observatorio del Teide, Tenerife, Canary Islands. The ChroTel has been developed by the Kiepenheuer-Institute in cooperation igh Altitude Observatory in Boulder, CO, USA. We acknowledge rvethesun.com and www.solarstation.ru for storing the data. This work used data provided by the MEDOC data and

References

Antonucci, E., Azzarelli, L., Casalini, P., & Cerri, S. 1977, Sol. Phys., 53,
Balmaceda, L. A., Solanki, S. K., Krivova, N. A., & Foster, S. 2009, J. Geo
Res.: Space Phys., 114,
Barata, T., Carvalho, S., Dorotovic, I., et al. 2018, Astron. Comput., 24, 70
Belkina, I. L., Beletskij, S. A., Gretskij, A. M., & Marchenko, G. P.
Kinematics Phys. Celest. Bodies, 12, 55
Berrilli, F., Ermolli, I., Florio, A., & Pietropaolo, E. 1999, A&A, 344, 965
Bethge, C., Peter, H., Kentischer, T. J., et al. 2011, A&A, 534, A105
Chapman, G. A., Cookson, A. M., & Dobias, J. J. 1997, ApJ, 482, 541
Chapman, G. A., Dobias, J. J., & Arias, T. 2011, ApJ, 728, 150
Chapman, G. A., Cookson, A. M., & Preminger, D. G. 2012, Sol. Phys., 27
Chatterjee, S., Banerjee, D., & Ravindra, B. 2016, ApJ, 827, 87
Chatterjee, S., Mandal, S., & Banerjee, D. 2017, ApJ, 841, 70
Chatzistergos, T. 2017, Analysis of Historical Solar Observations and Long-
Changes in Solar Irradiance PhD thesis (Uni-edition)
Chatzistergos, T., Ermolli, I., Solanki, S. K., & Krivova, N. A. 201
Coimbra Solar Physics Meeting: Ground-based Solar Observations i
Space Instrumentation Era, eds. I. Dorotovic, C. E. Fischer, & M. Te
(San Francisco), ASP Conf. Ser., 504, 227
Chatzistergos, T., Usoskin, I. G., Kovaltsov, G. A., Krivova, N. A., & So
S. K. 2017, A&A, 602, A69
Chatzistergos, T., Ermolli, I., Solanki, S. K., & Krivova, N. A. 2018a, A&A,
A92
Chatzistergos, T., Ermolli, I., Krivova, N. A., & Solanki, S. K. 2018
Long-term Datasets for the Understanding of Solar and Stellar Mag
Cycles, eds. D. Banerjee, J. Jiang, K. Kusano, & S. Solanki (Cambridge,
Cambridge University Press), IAU Symp., 340, 125
Chatzistergos, T., Ermolli, I., Falco, M., et al. 2019a, Il Nuovo Cimento, 42
Chatzistergos, T., Ermolli, I., Krivova, N. A., & Solanki, S. K. 2019b, A&A,
A69
Chatzistergos, T., Ermolli, I., Solanki, S. K., et al. 2019c, Sol. Phys., 294, 1
Chatzistergos, T., Ermolli, I., Solanki, S. K., et al. 2019d, A&A, 626, A114
Chatzistergos, T., Ermolli, I., Krivova, N. A., & Solanki, S. K. 2020, IOP J. P
Conf. Ser., 1548, 012,007
Curto, J. J., Solé, J. G., Genescà, M., Blanca, M. J., & Vaquero, J. M. 2016,
Phys., 291, 2587
Dizer, M. 1968, Sol. Phys., 3, 491
Dorotovic, I., Rybák, J., Garcia, A., & Journoud, P. 2010, 20th National
Physics Meeting, 20, 58
Ermolli, I., Berrilli, F., & Florio, A. 2003, A&A, 412, 857
Ermolli, I., Criscuoli, S., Centrone, M., Giorgi, F., & Penza, V. 2007, A&A,
305
Ermolli, I., Marchei, E., Centrone, M., et al. 2009a, A&A, 499, 627
Ermolli, I., Solanki, S. K., Tlatov, A. G., et al. 2009b, ApJ, 698, 1000
Ermolli, I., Krivova, N., & Solanki, S. K. 2010, in 38th COSPAR Scie
Assembly, COSPAR Meeting, 38, 133
Ermolli, I., Criscuoli, S., & Giorgi, F. 2011, Contrib. Astron. Obs. Skalnate P
41, 73
Ermolli, I., Matthes, K., Dudok de Wit, T., et al. 2013, Atm. Chem. Phys.
3945
Ermolli, I., Chatzistergos, T., Krivova, N. A., & Solanki, S. K. 2018, in L
term Datasets for the Understanding of Solar and Stellar Magnetic Cy
eds. D. Banerjee, J. Jiang, K. Kusano, & S. Solanki (Cambridge,
Cambridge University Press), IAU Symp., 340, 115
Fontenla, J. M., & Landi, E. 2018, ApJ, 861, 120
Galvez, R., Fouhey, D. F., Jin, M., et al. 2019, ApJS, 242, 7
Garcia, A., Sobotka, M., Klvana, M., & Bumba, V. 2011, Contrib. Astron.
Skalnate Pleso, 41, 69
Golovko, A. A., Golubeva, E. M., Grechnev, V. V., et al. 2002, Solar Variab
From Core to Outer Frontiers (ESA Publications Division), 506, 929
Gray, L. J., Beer, J., Geller, M., et al. 2010, Rev. Geophys., 48, 4001
Haigh, J. D. 2007, Liv. Rev. Sol. Phys., 4, 2
Hale, G. E. 1893, Mem. Soc. Spettr. It., 21, 68
Hale, G. E., & Ellerman, F. 1903, Publ. Yerkes Obs., 3, I.1
Hanaoka, Y. 2013, J. Phys. Conf. Ser., 440, 2041
Hanaoka, Y. 2016, Solar Observatory of NAOJ 2016, in Coimbra Solar Ph
Meeting: Ground-based Solar Observations in the Space Instrumentation

rk, L., Lee, H., et al. 2019, Nat. Astron., 1

Jeno, S., Maehara, H., et al. 2013, Data Sci. J., 12, WDS213

J., Belik, M., Klimeš, J. S., & Marková, E. 1999, in 8th SOHO op: Plasma Dynamics and Diagnostics in the Solar Transition Region ona, eds. J. C. Vial, & B. Kaldeich-Schü, ESA SP, 446, 375

L., Dettwiller, L., Audejean, M., Valais, M., & Ariste, A.L. 2019, 31, A55

Krivova, N., Wu, C. J., & Lean, J. 2016, Sol. Phys., 291, 2951

., Ulrich, R. K., Webster, L. S., et al. 2005, Mem. Soc. Astron. It., 76,

Srba, J., Gregorova, B., Exnerova, M., & Lenzova, N. 2014, System ultaneous Observation of Solar Flares in Spectral Lines of H-alpha I K

a, M., Solanki, S. K., & White, S. M. 2009, A&A, 497, 273

A., Carvalho, S., Barata, T., et al. 2019, Open Astron., 28, 165

J.-M., & Dalmasse, K. 2019, Sol. Phys., 294, 52

., Hochedez, J.-F., Irbah, A., et al. 2014, Sol. Phys., 289, 1043

., Corbard, T., Hauchecorne, A., et al. 2018, A&A, 616, A64

. 1965, Appl. Opt., 4, 1085

C., & Dodson, H. W. 1968, Sol. Phys., 5, 417

942, MNRAS, 102, 86

F., Marquette, W. H., Tritschler, A., & Denker, C. 2010, Astron. 331, 696

loon, Y.-J., Lee, J.-Y., et al. 2019, ApJ, 884, L23

Raju, K. P. 2018, MNRAS, 478, [illegible]

Rast, M. P., Ortiz, A., & Meisner, R. W. 2008, ApJ, 673, 1209

Shapiro, A. I., Solanki, S. K., Krivova, N. A., et al. 2017, Nat. Astron., 1,

Singh, J., & Ravindra, B. 2012, Bull. Astron. Soc. India, 40

Solanki, S. K., Krivova, N. A., & Haigh, J. D. 2013, ARA&A, 51, 311

Suo, L. 2020, Adv. Space Res., 65, 1054

Svalgaard, L., & Schatten, K. H. 2016, Sol. Phys., 291, 2653

Tlatov, A. G., & Tlatova, K. A. 2019, Geomag. Aeron., 59, 6

Tlatov, A. G., Pevtsov, A. A., & Singh, J. 2009, Sol. Phys., 255, 239

Tlatov, A. G., Dormidontov, D. V., Kirpichev, R. V., Pashchenko, M. Shramko, A. D. 2015, Geomag. Aeron., 55, 961

Vaquero, J. M., Gallego, M. C., & Acero, F. J. 2007, in The Phys Chromospheric Plasmas, eds. P. Heinzel, I. Dorotovic, & R. J. Rutten Conf. Ser., 368

Vogler, F., Brandt, P., Otruba, W., Pötzi, W., & Hanslmeier, A. 2008, Cen Astrophys. Bull., 32, 141

Waldmeier, M. 1968, Sol. Phys., 5, 423

Wöhl, H. 2005, Hvar Obs. Bull., 29, 319

Wu, C.-J., Krivova, N. A., Solanki, S. K., & Usoskin, I. G. 2018, A&A A120

Yeo, K.L., Krivova, N.A., & Solanki, S.K. 2017, J. Geophys. Res.: Space 2016JA023733

Zuccarello, F., Contarino, L., & Romano, P. 2011, Contrib. Astron. Obs. Sk Pleso, 41, 85

ppendix A: Processing of Kyoto and Yerkes data

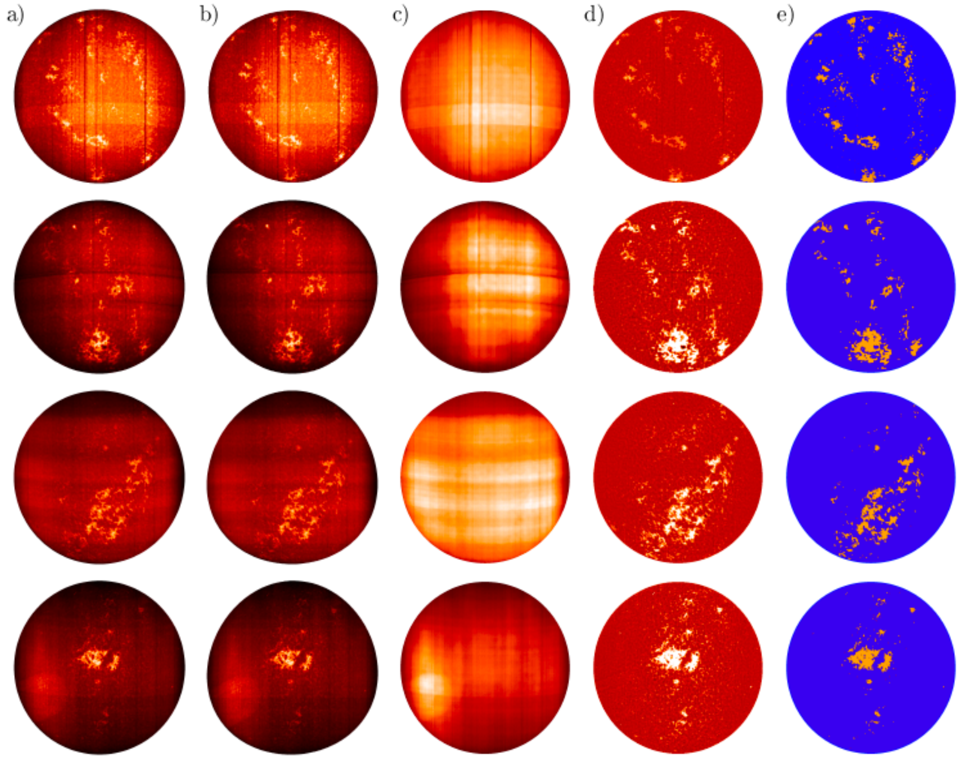

g. **A.1.** Examples of processing steps applied on Ky observations taken on 22/10/1937 (*first row*), 28/10/1939 (*second row*), 21/01/1959 (*thir*
v), and 30/04/1961 (*fourth row*). Columns are: original raw density image *(a)*, density image resampled to straighten the arcs *(b)*, compute
ckground of the original image *(c)*, photometrically calibrated and limb-darkening-compensated image *(d)*, and segmentation mask *(e)*. Th
v density images and the backgrounds are shown to the entire range of values within the disc, the calibrated images are shown in the rang
0.5, 0.5], while the masks show plage regions in orange and QS and network regions in blue. The images are not compensated for ephemeris.

ages from all sites that used spectroheliographs suffer from
efacts introduced by the motion of the slit of the spectrohe-
graph. Most of these follow the slit's shape, which is linear
almost all instruments. For the Ky and YR archives, how-
er, these artefacts appear to be curved rather than linear. To
ake things more complicated, there are linear artefacts roughly
rpendicular to the curved ones as well (see Fig. A.1), likely
roduced by other instrumental issues. The curved artefacts are
re evident in the Ky data than in YR ones and for that reason
focus on Ky data here, even though the same process was
plied on both series. To account for the curved artefacts in the
ta, we adopted the following processing.

During the pre-processing of the data, we identified the cen-
and the radius of the disc as well as the orientation and the
rvature of the arcs within each raw image. The identification of
linear and curved segments was initially done automatically.
e linear segments in most images are aligned with the frame
the photograph. The frame, however, is not always aligned
the digital image. Therefore, we applied Sobel filtering to
entify the frame and then determine the angle needed to align
linear segments vertically. The curved segments were iden-
ied by singling out bright or dark regions in the image after
was divided by a map constructed with a running window
edian filter with width of ten pixels.

However, both the linear and the curved segments are no
always clearly visible and the code was not always able t
detect them. For that reason, the results were afterwards man
ually inspected and corrected when deemed necessary. We iden
tify pixels belonging to the same arc and for each pixel n w
determine its horizontal distance from the left side of the image
y_n, and its vertical distance from the bottom of the image, x_n. I
order to get the parameters of the arcs, we fit a parabolic functio
of the form:

$$y_n = b_0 + b_1\,(x_n - b_2)^2\,, \qquad \text{(A.1}$$

where, b_0 and b_2 are the vertical and horizontal distances of th
centre of the parabola, while b_1 is its curvature. The values o
b_1, b_2 and the angle to orient the linear brightenings or darken
ings on the vertical direction were stored in the header of the ra
files, while b_0 was not stored as it has a different value for eac
arc. Furthermore, we make the assumption that all arcs can b
described with the same parabola with different offsets in the ver
tical direction. This is justified, unless there are other distortion
of the image affecting the shape of the artefacts. We also note tha
our processing can return consistent results with small deviation
in the determination of the curvature. The angle of the linear seg
ments is used at the beginning of the calibration process to rotat
the image so that the linear brightenings or darkenings are on th

ing a transformation of $y_{ij} = -b_1(x_{ij} - b_2)^2$, where y_{ij} and the distance in the vertical and horizontal direction of the i, el, respectively. After each fit in the horizontal direction, we the inverse transformation on the result of the fit, so to reince the curvature of the arcs. Hence, we apply the polynomial cross linear segments, but due to the aforementioned transation, the result follows the curvature of the arcs. The image ting after the first transformation is somewhat egg-shaped second column of Fig. A.1), while the circular shape of the s recovered after the inverse transformation. Both the direct ts inverse transformations were applied every time a polyal fit on the horizontal direction had to be performed. We that this transformation affects only the result of the fits on orizontal direction, the original image remained unchanged is procedure. In addition, we adapted the width of the runwindow median filter to be $R/20$ instead of $R/6$ which was for the processing of data from all the other datasets. Examof the processing applied to Ky data can be seen in Fig. A.1, ing that our processing could accurately remove the severe acts affecting the raw data. More such examples are shown atzistergos et al. (2020).

endix B: Assignment of datasets in the ackbone series

B.1 lists the various datasets used in this study and ackbone that they were assigned to. The annual coverage e datasets in the individual backbone series is shown in B.1–B.3.

which were not included in the RP1 backbone due to ins overlap.

Following Paper II, we split the Ar series at 25/0 the Mi series at 01/02/1966, the MW series at 21/08/1 01/01/1976, the Kh series at 01/01/1994, and the SP s 01/01/1963 to account for instrumental changes affec coherence of the series. Similarly, we split the BB s 01/07/1992 and 10/09/1996 (Naqvi et al. 2010), the Ka 24/11/2012, the SF1 series at 05/02/2002, and the SF2 28/07/1998 when the employed filters were replaced (C et al. 2011). We also split the ML series at 01/01/2005, prior to that date there were many instrumental issues denced by the log of the observations[3] (see also Vogl 2008). Due to the inhomogeneities of the ML dataset, from the data prior to 2005 had not been presented prio study. We also split the Co series at 01/01/1992 to accoun change of the grating system and 01/01/2008 when a CC era started being used for the regular observations. Simil split the MD1 series at 01/01/1919, 17/09/2002, and 15/ to account for instrumental changes, the introduction of camera, and the change in bandwidth used for the obser respectively. Finally, we split the Ki series at 2002 to acc the introduction of the CCD.

We merged the series by Ke[4] and YR[5] due to the low of recovered images from these datasets and the fact t were performed with the same telescope and spectrohel (Hale & Ellerman 1903). Similarly we merged the serie and WS. We will refer to these two series as Ke/YR and respectively.

---

[3] http://lasp.colorado.edu/media/projects/pspt_ PSPT_Final_Release_Notes.pdf

[4] The data were downloaded from http://peabody.ya collections

	Our series	Individual
Ar (before 25/05/1953)	Ko, MW	Ky, MD1, MM
Ar (after 25/05/1953)	Ko, MW	Ar, Ky, MD1, MM, Ro, SP
Ba	RP1	
BB (before 01/07/1992)	Ko	MD1, SP
BB (01/07/1992–10/09/1996)	Ko	MD1, SP
BB (after 10/09/1996)	RP1	
Br	RP1	
CT	Ko, MW	Ar, MD1, MM, Ro, SP
CL	RP1	
Co (before 01/01/1992)	Ko, MW	Ar, Ky, MD1, MM, Ro, SP
Co (01/01/1992–01/01/2008)	RP1	
Co (after 01/01/2008)	RP1	
Ka (before 24/11/2012)	RP1	
Ka (after 24/11/2012)	RP1	
Ke/YR	Ko	
Kh (before 01/01/1994)	Ko, MW	Ar, Ky, MM, Ro
Kh (after 01/01/1994)	RP1	
Ki (before 01/01/2002)	Ko, MW	Ar, Ky, MD1, MM, Ro, SP
Ki (after 01/01/2002)	RP1	
Ko	Ko, MW	Ar, Ky, MD1, MM, Ro, SP
KT	RP1	
KW	RP1	
Ky	Ko, MW	Ar, Ky, MD1, MM, Ro, SP
Ma	Ko, MW	Ar, Ky, MD1, MM, Ro, SP
ML (before 01/01/2005)	RP1	
ML (after 01/01/2005)	RP1	
MM	Ko, MW	Ar, Ky, MD1, MM, Ro, SP
MS	RP1	
MD1 (before 01/01/1919)	Ko	
MD1 (01/01/1919–26/09/2002)	Ko, MW	Ar, Ky, MD1, MM, Ro, SP
MD1 (27/09/2002–14/06/2017)	RP1	
MD1 (after 15/06/2017)	RP1	
MD2	RP1	
Mi1 (before 01/02/1966)	Ko, MW	Ar, Ky, MD1, MM, Ro, SP
Mi1 (after 01/02/1966)	Ko, MW	Ar, Ky, MD1, MM, Ro, SP
Mi2	RP1	
MW (before 21/08/1923)	Ko	MD1
MW (21/08/1923–31/12/1975)	Ko, MW	Ar, Ky, MD1, MM, Ro, SP
MW (after 31/12/1975)	Ko	MD1, MM, Ro, SP
PM	RP1	
PS	RP1	
Ro	Ko, MW	Ar, Ky, MD1, MM, Ro, SP
RP1	RP1	
RP2	RP1	
SF1 (before 05/02/1996)	Ko	MD1, SP
SF1 (after 05/02/1996)	RP1	
SF2 (before 28/07/1998)	RP1	
SF2 (after 28/07/1998)	RP1	
SP (before 01/01/1963)	Ko, MW	Ar, Ky, MD1, MM
SP (after 01/01/1963)	Ko, MW	Ar, Ky, MD1, MM, Ro, SP
Te	RP1	
UP	RP1	
VM	RP1	
WS/Sc	Ko, MW	Ar, Ky, MD1, MM, Ro, SP

olumns present: the name of the observatory and backbone to which it has been assigned in our composite series as well as the in
e series discussed in Sect. 4.

Fig. B.1. Annual coverage of datasets included in the RP1 backbone.

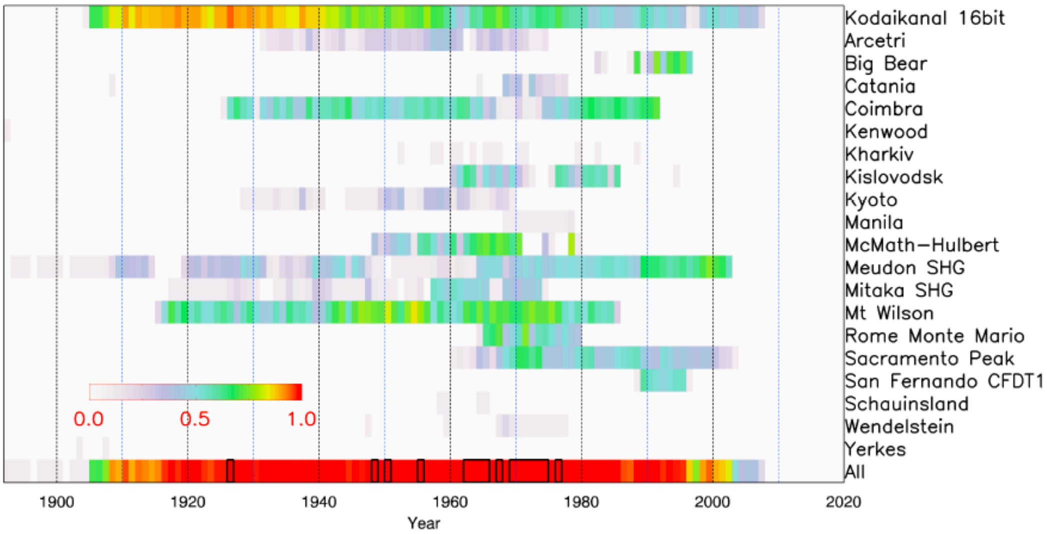

Fig. B.2. Annual coverage of datasets included in the Ko backbone.

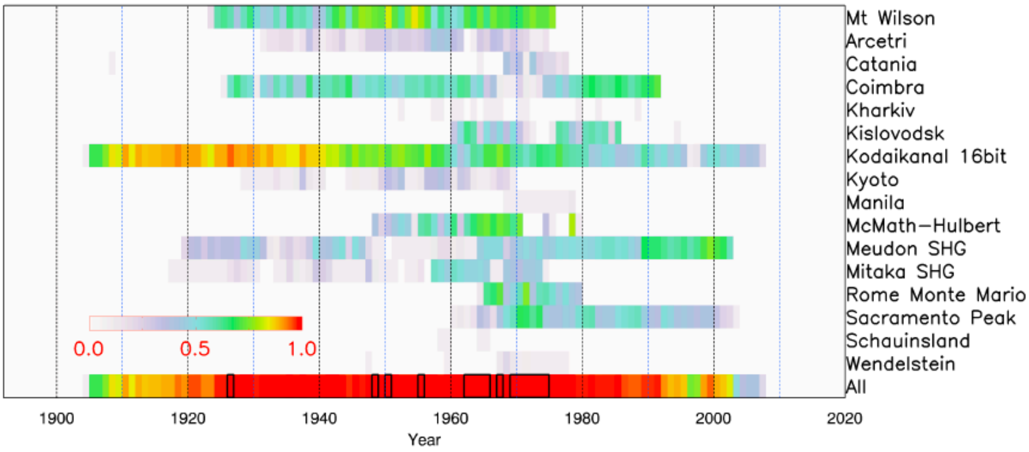

Fig. B.3. Annual coverage of datasets included in the MW backbone.